ARTICLES

Instabilities and singularities in Hele–Shaw flow

Raymond E. Goldstein
Department of Physics and Program in Applied Mathematics, University of Arizona, Tucson, Arizona 85721

Adriana I. Pesci
Department of Physics, University of Arizona, Tucson, Arizona 85721

Michael J. Shelley[a)]
The Courant Institute of Mathematical Sciences, New York University, New York, New York 10012

(Received 14 October 1997; accepted 2 July 1998)

A mechanism by which smooth initial conditions evolve towards a topological reconfiguration of fluid interfaces is studied in the context of Darcy's law. In the case of thin fluid layers, nonlinear PDEs for the local thickness are derived from an asymptotic limit of the vortex sheet representation. A particular example considered is the Rayleigh–Taylor instability of stratified fluid layers, where the instability of the system is controlled by a Bond number B. It is proved that, for a range of B and initial data ''subharmonic'' to it, interface pinching must occur in at least infinite time. Numerical simulations suggest that ''pinching'' singularities occur generically when the system is unstable, and in particular immediately above a bifurcation point to instability. Near this bifurcation point an approximate analytical method describing the approach to a finite-time singularity is developed. The method exploits the separation of time scales that exists close to the first instability in a system of finite extent, with a discrete spectrum of modes. In this limit, slowly growing long-wavelength modes entrain faster short-wavelength modes, and thereby, allow the derivation of a nonlinear evolution equation for the amplitudes of the slow modes. The initial-value problem is solved in this slaved dynamics, yielding the time and analytical structure of a singularity that is associated with the motion of zeros in the complex plane, suggesting a general mechanism of singularity formation in this system. The discussion emphasizes the significance of several variational principles, and comparisons are made between the numerical simulations and the approximate theory. © *1998 American Institute of Physics.* [S1070-6631(98)01810-8]

I. INTRODUCTION

Since the work of Plateau in the 19th century and continuing with Rayleigh's contributions, one focus in the study of natural patterns has been hydrodynamic instabilities. By and large, models of these phenomena were solved in their linearized form. These solutions have provided us with a great wealth of information such as characteristic length and time scales associated with the incipient patterns. However, it is clear that some of the most interesting situations occur beyond the point at which these linearized approximations break down. For example, linear theories are (usually) unable to provide us with finite time singularities. This fact alone renders them inaccurate at best and plain and simply wrong at worst. No linear theory can describe a phenomenon as familiar as the splitting of a drop of water. This is but one example of a more general question: How do smooth initial conditions evolve to produce finite-time singularities?

Of the many different systems that present finite-time singularities there is a whole class that can be formulated in the flux form

$$h_t + j_x = 0, \quad \text{with} \quad j = h(h_{xxx} + \cdots). \tag{1}$$

Equations of this type describe phenomena as diverse as interface motion in thin-film flow, Marangoni convection,[1] pattern formation in population dynamics,[2] the homogenized model of Type-II superconductors,[3] and the oxidation of semiconductor surfaces.[4]

Within this group we study here the case of the Rayleigh–Taylor (RT) instability of stratified fluid layers in Hele–Shaw flow.[5–7] This flow is described by Darcy's law, which is not only intrinsically interesting, but also of considerable importance by being a prototype of models of continuous media that display instabilities. Thus, it serves as a natural testing ground for methods of studying finite-time singularities. In this context, we give a complete derivation of a partial differential equation (PDE) that describes the Rayleigh–Taylor instability of thin fluid layers, starting from an exact vortex sheet formulation, the basic results of which were announced earlier.[6] This derivation provides a systematic justification for more phenomenological arguments used

[a)]Author to whom correspondence should be addressed. Telephone: 212-998-3284; Fax: 212-995-4121; Electronic mail: shelley@cims.nyu.edu

in related work,[8,9] and is based on an expansion in powers of the aspect ratio of the layer; truncation at second order gives what is known as ''lubrication theory.'' Here h is the layer thickness. The flux $j=hU$ in Eq. (1) has a velocity $U\sim -P_x$ arising from Darcy's law, and the pressure P is set by boundary conditions involving surface tension and gravity. In other contexts, the velocity has the more general form $\mathbf{U}\sim -h^m\nabla P$, such as in the spreading of drops ($m=2$). Such lubrication approximations have been the focus of a considerable body of subsequent work on the flow and rupture of thin films and the spreading of drops,[6–17] and provided the background for long-wave theories used to study the fissioning of axisymmetric[18–22] and planar jets.[23]

Two of the works based on the derived lubrication model (1) are of particular relevance here. First, Bertozzi and Pugh[14] analyze a class of lubrication-type PDEs which have a long-wave instability. This class includes the PDE [Eq. (9), below] that is the primary focus here. For this PDE they provide an *a priori* upper bound on $h_{\max}$, and prove that if h is positive then it is also smooth. Thus, smoothness can only be lost though a pinching singularity, i.e., $h\downarrow 0$. They also prove the global existence of a nonnegative ''weak'' solution, a result that does not preclude the formation of pinching singularities. They conjecture that one scenario for the ultimate state of the system is relaxation to a set of compactly supported positive regions, connected by zero sets. Second, Almgren, Bertozzi, and Brenner[12] have studied the ''unforced'' lubrication equation, which is a special case of the system we consider, and which has no long-wave instability. For a special class of smooth initial data for h, they observe numerically and analyze three types of pinching singularities, two of which were found earlier[7,9–11] and are central here.

We obtain variational principles that allow us to study the stability of nontrivial positive steady-states. For the Rayleigh–Taylor case, these same variational principles also allow us to prove that PDE must develop a pinch, or $h\downarrow 0$, in at least infinite time, for a range of bond number and initial data that is subharmonic to its associated (nondimensional) length-scale. If a pinch occurs in finite time, then h must develop a singularity. Our numerical results suggest that the approach to a pinch is generic when the system is unstable. We also find strong numerical evidence to support a finite time singularity in the PDE immediately above the bifurcation to instability. Finally, we develop an approximate analytical technique to solve the initial-value problem, based on a separation of time scales near this onset of instability. This analysis involves the merging of two previously independent ideas from dynamical systems theory: The coupling of slaved small spatial scales to low-mode dynamics as in the reduction of dissipative PDEs to inertial manifolds,[24] and the description of interface motion in terms of zeros or singularities in the complex plane.[25] Comparison of this approximate theory with our numerical simulations show very good agreement until quite close to the apparent singularity time, when the assumptions underlying the theory break down, and the simulations show a divergence from its predictions. Nonetheless, we do find that the ultimate spatial structure of the singularity suggested by this analysis agrees very well with that found in our numerical simulations.

II. THE EQUATIONS OF MOTION

In this section we derive the equation of motion of interfaces bounding a thin layer of fluid in a Hele–Shaw cell. The necessary mathematical formalism is best illustrated by considering first the motion of a single interface Γ. The two fluids which it separates are labeled 1 and 2, and likewise for their densities ρ and viscosities μ, and are assumed to obey Darcy's law

$$\mathbf{v}_j=-\frac{b^2}{12\mu_j}(\nabla P_j-\rho_j\mathbf{F}) \quad \text{and} \quad \nabla\cdot\mathbf{v}_j=0. \tag{2}$$

Here b is the gap width of the cell, $\mathbf{v}_j$ and P_j are the velocity and pressure in each fluid ($j=1,2$), and $\mathbf{F}=-\nabla\phi$ is a body force (e.g., gravitational force). Each pressure P_j is harmonic and acts as a velocity potential. We define $A=(\mu_1-\mu_2)/(\mu_2+\mu_1)$ as the Atwood ratio for the viscosities, $\Delta\rho=\rho_1-\rho_2$, and $\theta=6(\mu_1+\mu_2)/b^2$.

The boundary conditions at the interface Γ are (i) the kinematic condition

$$(\mathbf{v}_1-\mathbf{v}_2)\cdot\mathbf{n}|_\Gamma=0, \tag{3}$$

and (ii) the Young–Laplace condition

$$P_1-P_2=-\Theta\kappa, \tag{4}$$

where $\mathbf{n}$ is the upward normal to Γ, Θ is the surface tension, and κ is the curvature of Γ. In addition, Γ is required to move with the normal fluid velocity.

We assume that Γ is a graph $(x,h(x,t))$, that is, its height $h(x,t)$ is single valued in x. Since Γ moves with fluid in the normal direction, $h(x,t)$ obeys

$$h_t(x,t)=\overline{v}-\overline{u}h_x(x,t), \tag{5}$$

where $(\overline{u},\overline{v})$ is the mean fluid velocity at Γ.

The dynamics of Γ can be given self-consistently by using a vortex sheet representation for the fluid velocity.[5,26,27] That is, $\overline{\mathbf{U}}=(\overline{u},\overline{v})$ can be expressed entirely in terms of $h(x,t)$ and its derivatives

$$\overline{\mathbf{U}}[\gamma]=\frac{1}{2\pi}P\int_{-\infty}^{+\infty}dx'\,\gamma(x')\,\frac{(h(x')-h(x),x-x')}{(x-x')^2+(h(x)-h(x'))^2}, \tag{6}$$

where the vortex sheet strength γ satisfies a Fredholm integral equation of the second kind

$$\gamma+2A_\mu\overline{\mathbf{U}}[\gamma]\cdot(1,h_x)=\frac{1}{\theta}\{\Theta\kappa_x+\Delta\rho\nabla\phi(x,h(x))\cdot(1,h_x)\}. \tag{7}$$

For the problems of interest here, this integral equation has a unique solution.

This framework is readily extended to the case of two interfaces bounding a layer of fluid and yields a pair of coupled equations analogous to (6) and (7). We consider the simplest case, shown in Fig. 1, where the interfaces are mirror images with respect to the x axis. This is equivalent to the case of a single interface bounding a fluid layer against a wall.

To gain insight into this mathematically complicated system, we simplify the equations of motion by considering

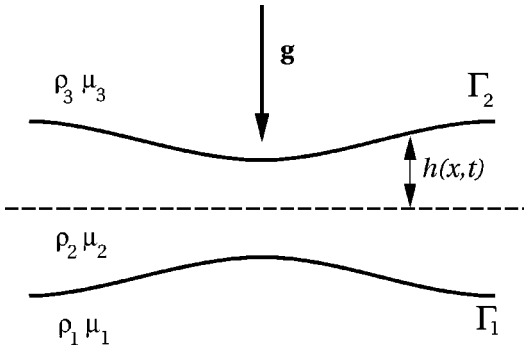

FIG. 1. A schematic of a thin layer of fluid, trapped between two others, in the Hele–Shaw cell.

a thin fluid layer. Let the fluid layer have length L and a mean thickness w. We consider L as scaling with the lateral width of the cell. We define a thin fluid layer as one for which $\epsilon \equiv w/L \ll 1$, and expand the full system in ϵ. We will see that retaining only the leading-order terms of this expansion yields the so-called lubrication approximation.

The essential aspects of the expansion procedure are as follows. We rescale x with L, h with w, and t with $T = \Theta/L^3\theta$ (γ scales naturally then with L/T). The expansion in ϵ of the vortex sheet integrals, which depend on h, h_x, and $\kappa = h_{xx}/(1+h_x^2)^{3/2}$, is very involved; the details of the method are given in Appendix A, and rely on techniques developed in Ref. 28.

We consider two cases. The first consists of a fluid layer against a wall, with the gravitational force acting perpendicular to the layer ($\mathbf{F} = -g\hat{\mathbf{y}}$). This leads to a Rayleigh–Taylor instability. The second case is that of a gravity driven jet, falling through another fluid. Here, the gravitational force is parallel to the layer ($\mathbf{F} = g\hat{\mathbf{x}}$). Unless stated otherwise, for the remainder of the paper we consider 2π-periodic solutions to the equations of motion.

A. The Rayleigh–Taylor instability

By expanding to second order in ϵ, we find that h is governed by the local PDE

$$(1-A_\mu)h_t = -\epsilon\partial_x(h(h_{xxx}+Bh_x)). \tag{8}$$

By defining a rescaled time $t' = \epsilon t/(1-A_\mu)$ (and immediately dropping the $'$), we have

$$h_t = -\partial_x(h(h_{xxx}+Bh_x)). \tag{9}$$

Here the Bond number

$$B = \frac{g\Delta\rho L^2}{\Theta}, \tag{10}$$

measures the relative importance of buoyancy to the restoring force of surface tension. When $B=0$, we recover the equation studied in earlier works.[8,9]

It is useful to compare the linear stability of a flat interface $h(x)=\bar{h}$ in the lubrication approximation with the exact vortex sheet calculation. In the lubrication approximation, the growth rate of a disturbance of wave number k is

$$\sigma_k = -\bar{h}(k^4 - Bk^2), \tag{11}$$

as opposed to the exact result

$$\sigma_k = -\frac{1}{2\epsilon}(|k|^3 - B|k|)(1-e^{-2|k|\epsilon\bar{h}}). \tag{12}$$

Equation (11) follows from Eq. (12) by expansion in small $k\epsilon\bar{h}$, as the lubrication approximation is a long-wavelength theory.

The relation (11) gives the familiar result that the fluid is unstably stratified if $B>0$, i.e., the heavier fluid is on top. This Rayleigh–Taylor instability is suppressed at small length scales by surface tension.

B. The gravity-driven jet

Again expanding to second order in ϵ, and rescaling time as above, we find that h is governed by the nonlocal PDE

$$h_t(x,t) - \frac{B}{\epsilon}h_x = -\partial_x\left\{h\left(h_{xxx} - B\frac{\mu_1}{\mu_2}\mathscr{H}[h_x]\right)\right\}, \tag{13}$$

where $\mathscr{H}$ represents the Hilbert transform

$$\mathscr{H}[f] = \frac{1}{\pi}P\int_{-\infty}^{+\infty}dx'\,\frac{f(x')}{x-x'}. \tag{14}$$

The nonlocal term in (13) is absent when there is no outer fluid, resulting in the simpler local jet dynamics

$$h_t(x,t) - \frac{B}{\epsilon}h_x = -\partial_x(hh_{xxx}). \tag{15}$$

In either case, the term $(B/\epsilon)h_x$ arises only because of time being scaled upon ϵ [as in Eq. (9)]. This term is neutral within the dynamics and can be removed by a change-of-frame (at least for periodic boundary conditions).

Once again, the linearization of the full lubrication theory result (13) about a jet of mean thickness $\bar{h}$ yields the long-wavelength limit of the exact result from the vortex sheet formulation. The growth rate from (13) is

$$\sigma_k = i\frac{B}{\epsilon}k + iBk\frac{\mu_1}{\mu_2}\bar{h}|k| - \bar{h}k^4. \tag{16}$$

Thus the density stratification, regardless of the sign of B, leads only to linearly dispersive waves damped by the surface tension.

The equations of motion (9), (13), and (15) are in the form of a conservation law for h

$$h_t + j_x = 0, \quad j = hU, \tag{17}$$

where j is a current and U is the mean velocity given by Darcy's law. It follows from this form that if h vanishes anywhere in finite time there is a singularity in the velocity gradient U_x.[8]

III. VARIATIONAL PRINCIPLES AND THEIR CONSEQUENCES

The equations of motion for both the Rayleigh–Taylor problem (9) and the local jet dynamics (15) have the variational form

$$h_t = -\partial_x\left\{h\partial_x\left(\frac{\delta\mathscr{T}}{\delta h}\right)\right\}. \tag{18}$$

The characteristic velocity

$$U \equiv -\partial_x\left(\frac{\delta \mathscr{F}}{\delta h}\right), \tag{19}$$

is the gradient of a generalized pressure, according to Darcy's law. It follows from (18) and (19) that $\mathscr{F}$ decreases monotonically in time

$$\mathscr{F}_t = -\int_0^{2\pi} dx h U^2, \tag{20}$$

provided the width h is non-negative.

The functional that generates Eq. (9) from (18) is

$$\mathscr{F}_{\mathrm{RT}}[h] = \tfrac{1}{2}\int_0^{2\pi} dx\{h_x^2 - B(h^2 - \overline{h^2})\}$$

$$= \tfrac{1}{2}\sum_{k\neq 0} (k^2 - B)|\hat{h}_k|^2, \tag{21}$$

where $\hat{h}_k$ is the kth Fourier amplitude of h. Note that when $B<1$, $\mathscr{F}_{\mathrm{RT}}$ is strictly positive, but otherwise is of indefinite sign. For the jet dynamics (15) the energy functional is

$$\mathscr{F}_{\mathrm{jet}}[h] = \int_0^{2\pi} dx\left\{\frac{1}{2} h_x^2 + \frac{B}{\epsilon} hx\right\}. \tag{22}$$

In both cases, the term $(\frac{1}{2})h_x^2$ represents the excess arclength of a curved interface, while the contribution proportional to B is the potential energy of the fluid layer in the gravitational field. This second term is invariant in time, and so does not contribute to the evolution of the energy.

A quite different, but very useful, quantity is the entropy of the system, defined as

$$\mathscr{S}[h] = -\int_0^{2\pi} dx f(x) \ln f(x), \tag{23}$$

where $f = h/\overline{h}$. It satisfies $\mathscr{S} \leqslant 0$, and achieves its upper bound only for the flat interface $h \equiv \overline{h}$.

For the Rayleigh–Taylor problem, the entropy evolves in time according to

$$\mathscr{S}_t = \frac{1}{\overline{h}}\int_0^{2\pi} dx (h_{xx}^2 - B h_x^2)$$

$$= \frac{1}{2}\sum_{k\neq 0} k^2(k^2 - B)|\hat{h}_k|^2. \tag{24}$$

Again, for $B>1$, this quantity is indefinite in sign, while for $B<1$, $\mathscr{S}$ increases monotonically.

For $B=0$ with periodic boundary conditions, Bertozzi and Pugh[13] have used estimates based in part upon the entropy to prove the global existence of a weak solution, and ultimate relaxation of h to a flat state. The entropy also plays a central role in their more recent work on unstable lubrication type equations[14] (as discussed in the Introduction).

For the gravity-driven jet, the result is quite different. Because the transform $\mathscr{H}$ is a skew-symmetric operator, explicit dependence upon B in the entropy evolution is lost. We find that

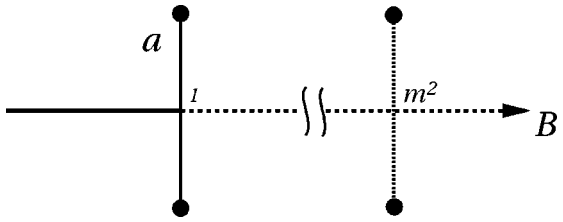

FIG. 2. Bifurcation diagram showing stable (solid) and unstable (dashed) solution branches as a function of bond number. The solid circles represent maximum amplitudes for positive h.

$$\mathscr{S}_t = \frac{1}{\overline{h}}\int_0^{2\pi} dx h_{xx}^2. \tag{25}$$

Now the entropy derivative is completely definite in sign, and the entropy is monotonically increasing.

These variational principles lead very directly to several results.

A. Steady states for the stratified layer

For the unstably stratified layer, the variational principle allows an enumeration of possible steady states. Here, we discuss smooth steady states and their stability.

Let $h_0(x)$ be a smooth and positive, 2π-periodic steady state to Eq. (9). Then, by Eq. (20), $h_0(x)$ must satisfy $U \equiv 0$, or equivalently, h_0 must be in the null space of the skew-symmetric linear operator $\mathcal{L}_B = \partial_{xxx} + B\partial_x$. For $B \leqslant 0$, only the flat equilibrium, $h_0 \equiv \overline{h}$, is possible. However, for $B>0$, this requirement gives two possibilities, either

(i) $h_0 \equiv \overline{h}$,

or, for $B = m^2$, m an integer,

(ii) $h_0 = \overline{h}(1 + a\cos\sqrt{B}x)$.

Here a is an undetermined constant that satisfies $a<1$. These are the only possible smooth and positive steady states. While terms involving $\sin\sqrt{B}x$ are also allowed, they can be subsumed into the form (ii) above.

Figure 2 shows a bifurcation diagram of these steady states, as a function of the bond number B. The parameter a is a convenient amplitude. The stability associated with each branch is indicated (solid is stable, dashed is unstable). That the branches bifurcating from the flat state do not bend with B follows directly from U being a linear operator upon h. This is a nongeneric behavior, which we will use later to our advantage. The linearity of U itself follows from the expansion of the curvature terms in the vortex sheet strength γ in the derivation of the lubrication approximation.

We can also find a set of weak solutions by knitting together the cosinusoidal solutions with zero sets. These weak solutions are the time independent solutions of the full equation of motion for the interface and are given by:

$$h = \begin{cases} h_0(1+\cos\sqrt{B}x) & |x| \leqslant \pi/\sqrt{B} \\ 0 & \pi/\sqrt{B} \leqslant |x| \leqslant \pi, \end{cases} \tag{26}$$

where h_0 is an arbitrary constant that sets the maximum height of the interface. This same set of solutions could be obtained by using the variational principles for the energy functional

$$\tilde{\mathscr{F}} = \int_0^{2\pi} dx\{\tfrac{1}{2}h_x^2 + \tfrac{1}{2}Bh^2\} - \lambda \int_0^{2\pi} dx h, \tag{27}$$

since the weak solutions for the equations of motion are its minimizers. The energy of these weak solutions is

$$\mathscr{F} = -\pi h_0^2 B^{3/2}. \tag{28}$$

While we have not been able to prove it, we suspect that such weak equilibria are stable. Numerical solutions of a ''regularized'' PDE, that allows evolution past a putative singularity time, show relaxation to nonoverlapping distributions of these solutions.[29] This agrees with the conjecture of Bertozzi and Pugh,[14] and agrees with their simulations for a related lubrication equation.

1. The stability of the smooth steady states

From Eq. (11), it is clear that the flat equilibrium is stable for $B \leqslant 1$ and unstable for $B > 1$. The stability of the nontrivial steady states, for $B = m^2$, is likewise not difficult to ascertain. Let $h_0 = h(1 + a\cos mx)$, and $h = h_0 + \epsilon\zeta$, with $\epsilon \ll 1$ and $\langle \zeta \rangle = 0$. The linearized evolution about h_0 is given by

$$\zeta_t = -\partial_x(h_0 \mathscr{L}_{m^2}\zeta). \tag{29}$$

Since ζ is periodic and of zero mean, it can be represented as the derivative of another periodic and zero mean function, that is, $\zeta = \eta_x$, with $\langle \eta \rangle = 0$. The evolution is then rewritten as

$$\eta_t = -h_0 \mathscr{L}_{m^2}\eta_x. \tag{30}$$

Since h_0 lies in the null space of $\mathcal{L}_{m^2}$, $\langle \eta \rangle = 0$ is preserved by this evolution. We define the (squared) norm as

$$\mathscr{E} = \frac{1}{2}\int_0^{2\pi} \frac{\eta^2(x,t)}{h_0(x)}\, dx, \tag{31}$$

whose time derivative satisfies

$$\mathscr{E}_t = -\int_0^{2\pi} dx(\eta_{xx}^2 - m^2\eta_x^2) = -\sum_k k^2\rho_k |\hat{\eta}_k|^2, \tag{32}$$

where $\rho_k = k^2 - m^2$ and $\hat{\eta}_k$ are the Fourier amplitudes of η. It is unclear whether there exists a straightforward physical interpretation of the norm $\mathscr{E}$ as defined above. However, $\mathscr{E}_t$ is clearly the equivalent of the functional $\mathscr{F}$ introduced in Eq. (18) for the full equations of motion. And so, $\mathscr{E}_{tt}$ satisfies

$$\mathscr{E}_{tt} = 2\int_0^{2\pi} dx h_0(\mathscr{L}_{m^2}\eta_x)^2 \geqslant 0. \tag{33}$$

This yields the following inequality:

$$\mathscr{E}_{tt} \geqslant C\int_0^{2\pi} dx(\mathscr{L}_{m^2}\eta_x)^2 = C\sum_k k^4\rho_k^2 |\hat{\eta}_k|^2, \tag{34}$$

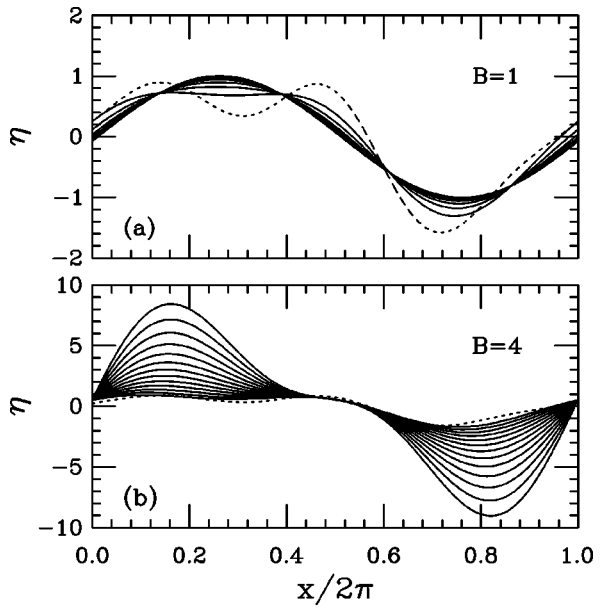

FIG. 3. Illustrations of the effect of bond number on the stability of steady states under perturbations η, with a common initial condition (dashed). (a) $B=1$: Stable. (b) $B=4$: Unstable.

where $C = 2\min_x h_0(x) > 0$. Since ρ_k is an integer for $B = m^2$, we have that $k^4\rho_k^2 \geqslant \pm k^2\rho_k$, which immediately yields the two inequalities

$$\mathscr{E}_{tt} \geqslant \pm C\mathscr{E}_t, \quad \text{or} \quad \mathscr{E}_t \geqslant e^{\pm Ct}\mathscr{E}_t(0). \tag{35}$$

These expressions will allow us to understand the stability of the solutions to the evolution equations for different values of the Bond number B.

a. $B = m^2 = 1$. The steady state h_0 is stable in the sense that a perturbation η decays into the null-space of $\mathcal{L}_1$.

For $m = 1$, Eq. (32) implies $\mathscr{E}_t \leqslant 0$, and that $\mathscr{E}_t = 0$ if and only if η is entirely in the null space of $\mathcal{L}_1$ (in this latter case, η is a steady state solution). Now, making use of the inequalities we find the relationship

$$0 \geqslant \mathscr{E}_t \geqslant \mathscr{E}_t(0)e^{-Ct}, \tag{36}$$

where $\mathscr{E}_t(0) \leqslant 0$. This means that $\mathscr{E}_t \to 0$ as $t \to \infty$ which in turn implies that h_0 is a stable equilibrium.

As an example the upper graph in Fig. 3 shows, for $B = 1$, the evolution of a multimode initial condition for η, as it relaxes to the null space of $\mathcal{L}_1$. This behavior reflects quite well that observed in numerical simulations of the full PDE.

b. $B = m^2 > 1$. The steady state h_0 is unstable to (at least) subharmonic perturbations. The second inequality in Eq. (36) gives

$$\mathscr{E}_t \geqslant \mathscr{E}_t(0)e^{Ct}. \tag{37}$$

If we consider an initial condition for η occupying only Fourier modes with $1 \leqslant |k| < m$ (i.e., modes subharmonic to h_0), then from Eq. (32) (which yields $\mathscr{E}_t(0) > 0$) and the bound above we deduce that $\mathscr{E}_t$ will grow at least exponentially.

The lower graph in Fig. 3 shows the growth of η, predominantly in the $k = 1$ mode, from a multimode initial condition for η with $B = 4$. Eventual instability seems generic also for initial conditions for which $\mathscr{E}_t$ is initially negative, and to which the instability arguments above do not directly apply. While an initial decay of $\mathscr{E}$ towards the null space of $\mathscr{L}_{m^2}$ may be observed, mode coupling through the variable

coefficient nature of the PDE (30) leads to an excitation of the subharmonic modes, and to eventual growth.

Finally we note that for the dynamics of the gravity driven jet the evolution of the entropy as defined in Eq. (25) precludes the existence of any nontrivial, periodic steady states.

B. Touchdown of the interface

The usefulness of the variational principle that governs these motions is not just limited to the study of linear stability. It can also be used to prove that for the full system (as opposed to the linearized version) there are initial data which will give rise to pinches, at least in infinite time. As was important in the previous section in the demonstration of linear instability of steady states for $B>1$, this initial data is again subharmonic to $\sqrt{B}$.

Consider the energy functional for the Rayleigh–Taylor PDE

$$\mathscr{F}=\tfrac{1}{2}\int_0^{2\pi} dx\{h_x^2-B(h^2-\overline{h^2})\}=\sum_{k\geqslant 1}\rho_k|\hat{h}_k|^2, \tag{38}$$

and its time derivative

$$\mathscr{F}_t=-\int_0^{2\pi} dx h(h_{xxx}+Bh_x)^2. \tag{39}$$

If $h_{\min}(t)=\min_\infty h(x,t)$, then we obtain directly

$$\begin{aligned}\mathscr{F}_t &\leqslant -h_{\min}\int_0^{2\pi} dx(h_{xxx}+Bh_x)^2,\\ &=-h_{\min}\sum_{k=-\infty}^{+\infty} k^2\rho_k^2|\hat{h}_k|^2.\end{aligned} \tag{40}$$

It can be shown that for $|k|\geqslant 1$ and $B\geqslant 2$, the inequality $k^2\rho_k^2>-\rho_k$ is satisfied. Equation (40) then directly yields $\mathscr{F}_t\leqslant 2h_{\min}(t)\mathscr{F}$, which can be transformed upon application of the Gronwall inequality into

$$\mathscr{F}(t)\leqslant\exp\left(2\int_0^t ds\, h_{\min}(s)\right)\mathscr{F}(0). \tag{41}$$

As has been proved by Bertozzi and Pugh,[14] the only singularity that can be realized by the equation of motion (9) is one associated with $h\downarrow 0$. We now assume that such an event does not occur at a finite time. In this circumstance it has also been proved in Ref. 14 that there is the global existence of a smooth solution, which we also henceforth assume. Then as $t\to\infty$ the function

$$\int_0^t ds\, h_{\min}(s), \tag{42}$$

must be either finite or infinite. Assume the latter, as would be the case when $h_{\min}$ is strictly bounded away from zero.

We show now that this assumption implies that h must pass through zero at a finite time. Consider initial data which is subharmonic to $\sqrt{B}$, giving $\mathscr{F}(0)<0$. Then

$$\lim_{t\to\infty}\mathscr{F}(t)\to-\infty. \tag{43}$$

For simplicity, we restrict B to the values $2\leqslant B<4$, so that $k=1$ is the only mode that is subharmonic to $\sqrt{B}$. Thus, in Eq. (38) the contributions of the Fourier modes can be separated into positive and negative, yielding

$$\mathscr{F}=-(B-1)|\hat{h}_1|^2+\sum_{k\geqslant 2}\rho_k|\hat{h}_k|^2, \tag{44}$$

and negativity of $\mathscr{F}$ gives immediately that

$$\sum_{k\geqslant 2}\rho_k\frac{|\hat{h}_k|^2}{|\hat{h}_1|^2}<B-1. \tag{45}$$

From Eq. (43) it follows that that the first term of Eq. (44), which is the only negative contribution and measures the subharmonic amplitude, must diverge and so $|\hat{h}_1|^2\to\infty$ as $t\to\infty$.

Now observe that $h(x,t)$ itself is given by

$$\begin{aligned}h(x,t)&=\overline{h}+\hat{h}_1e^{ix}+\hat{h}_1^*e^{-ix}+\sum_{|k|\geqslant 2}\hat{h}_ke^{ikx}\\ &=\overline{h}+|\hat{h}_1|\left(2\cos(x+\phi)+\sum_{|k|\geqslant 2}\frac{\hat{h}_k}{\hat{h}_1}e^{ikx}\right)\\ &=\overline{h}+|\hat{h}_1|g(x,t),\end{aligned} \tag{46}$$

where $e^{i\phi}=\hat{h}_1/|\hat{h}_1|$. The function $g(x,t)$ can be uniformly bounded in both x and t since

$$\left|\sum_{|k|\geqslant 2}\frac{\hat{h}_k}{\hat{h}_1}e^{ikx}\right|<2\sqrt{B-1}\left(\sum_{k\geqslant 2}\frac{1}{\rho_k}\right)=M_B. \tag{47}$$

This inequality follows from the Hölder inequality and inequality (45). M_B is known in closed form, and is finite except when $B=m^2$, m integer. For a small range of $B(2\leqslant B\leqslant 2.075)$, $M_B<2$. This implies that $\tilde{g}(t)\leqslant M_B-2<0$, where $\tilde{g}=\min_x g$. As $\hat{h}_1$ diverges, this implies then that $h(x,t)$ becomes negative in a finite time, i.e., a pinch.

We extend this conclusion to $2\leqslant B<4$ by a straightforward argument using

$$\begin{aligned}&\text{(i)}\quad \int_0^{2\pi} dx g(x,t)=0,\\ &\text{(ii)}\quad \int_0^{2\pi} dx g^2(x,t)=2+\sum_{|k|\geqslant 2}\left|\frac{\hat{h}_k}{\hat{h}_1}\right|^2\geqslant 2\ \text{ and}\\ &\text{(iii)}\quad |g(x,t)|\leqslant 2+M_B.\end{aligned} \tag{48}$$

Without loss of generality, assume that $\overline{h}=1$. Then there is a time $T\geqslant 0$ for which $\min_x|\hat{h}_1(t)|g(x,t)\leqslant -1$, i.e., pinching. To see this, assume that there is not such a time. Then given any ϵ, there is a time T_ϵ such that $0\geqslant\tilde{g}\geqslant-\epsilon$ for $t\geqslant T_\epsilon$. Then property (i) implies that

$$\int_0^{2\pi} dx|g|\leqslant 4\pi\epsilon, \tag{49}$$

which with property (iii) implies

$$\int_0^{2\pi} dx|g|^2\leqslant 4\pi\epsilon(2+M_B). \tag{50}$$

But this contradicts property (ii) for ϵ chosen sufficiently small.

Thus, the hypothesis of no finite time pinching is contradicted, and it must be that

$$\int_0^\infty ds h_{\min}(s) < \infty. \tag{51}$$

That is, if there is no finite time pinching, $h_{\min}$ must vanish faster than t^{-1}.

There are a few important points to be noted:

(i) These arguments can be extended to other ranges of B by simple rescalings of the equation. However, it would be most useful to extend these arguments to the range $1<B<2$, where the Gronwall inequality we have used here does not hold. Numerical experiments indicate nonetheless that pinching occurs generically in this range of B as well, and singularity formation there is the object of an approximate theory given in Sec. V.

(ii) There are two other constraints on h that can be derived. First, an isolated minimum $h_{\min}(t)$ itself obeys the flux equation

$$\frac{d}{dt} h_{\min}(t) = -h_{\min}(t) U_x(X(t),t), \tag{52}$$

where $X(t)$ tracks the location of the minimum of h. Then if there is no finite time pinching, we formally integrate this equation and apply Eq. (51), to obtain

$$\int_0^\infty \exp\left(-\int^s ds U_x(X(s),s) \right) < \infty. \tag{53}$$

Second, the same arguments can be applied to

$$h_m(t) = \frac{\int_0^{2\pi} dx h U^2}{\int_0^{2\pi} dx U^2}, \tag{54}$$

and which bounds $h_{\min}$ from above, to conclude also that

$$\int_0^\infty ds h_m(s) < \infty, \tag{55}$$

if there is no finite time pinching.

IV. INSTABILITIES, BIFURCATIONS, AND SINGULARITIES

In this section, we present simulations of the evolution of the full equation of motion in the lubrication approximation for the Rayleigh–Taylor problem (9). These simulations indicate that, at least for $B>1$, finite-time pinching singularities are generic. Further, as the bond number is increased, there is a change in both the form and the number of singularities produced.

A. Numerical methods

The simulations use pseudo-spectral collocation methods, both uniform and adaptive in space, and implicit in time to control the high-order stability constraints. The PDE has the form

$$h_t = -\partial_x (h \mathscr{L} h),$$

with $\mathscr{L}$ a linear operator. A simple implicit, second-order treatment of this PDE is the mixed Crank–Nicholson differencing

$$\frac{h^{n+1}-h^n}{\Delta t} = -\partial_x \left(\frac{1}{2} (h^n \mathscr{L} h^{n+1} + h^{n+1} \mathscr{L} h^n) \right). \tag{56}$$

We find no high order time-step constraint arising from this implicit differencing.

For evolution that is not yet near a singularity, the operator $\mathscr{L}h$ is typically evaluated on a uniform mesh using the Discrete Fourier Transform (DFT), and the quadratic nonlinearities are evaluated pseudo spectrally. Near an incipient singularity, we introduce a smooth and graded mesh that is reformed periodically, and that collapses as the singularity is approached. This amounts to a periodic change of variable, where the new spatial variable y satisfies

$$\frac{x_y}{\sqrt{h}} = \frac{1}{2\pi} \int_0^{2\pi} \frac{dx}{\sqrt{h}}.$$

It is motivated by the observation that the observed pinching singularities are usually close to assuming a local scaling form $h \sim \zeta(t)^2 H(\eta)$, where $\eta = (x-x_p)/\zeta$, and ζ is a collapsing length scale. Then, locally to the point of pinching, $x_\eta = \zeta \sim \sqrt{h}$, and so y is such a scaling variable in the neighborhood of the singularity. The constant on the right hand side (rhs) is chosen to enforce periodicity of the mapping. We take this approach because it required relatively minor changes to the uniform mesh spectral code. In either case, this change of variable simply introduces metric factors into the evaluation of spatial derivatives, and produces at the next time step a full system of equations for h^{n+1} on the mesh, which we write as

$$\mathbf{A}\mathbf{h}^{n+1} = \mathbf{r}. \tag{57}$$

This system is solved using the iterative linear solver GMRES (see Ref. 30), which requires only the result of matrix multiplications by $\mathbf{A}$ upon a vector. This is accomplished in $O(N \ln N)$ operations by pseudo-spectral collocation, where N is the number of grid points. The iteration is accelerated by a finite difference based preconditioner, and the first guess at each time step is given by an extrapolation of solutions at previous time steps. Convergence to the solution requires typically only a few iterations.

An alternative approach is a self-similar adaptive mesh scheme, developed by Bertozzi[10] and others, which uses finite differences. It is especially effective in resolving the fine structure of symmetric singularities, where round-off error can be reduced by special choices for mesh point locations.

B. Numerical results

The initial condition chosen is a perturbation of the flat interface:

$$h(x,t=0) = \bar{h}(1 + a \cos x), \quad 0 \leqslant x \leqslant 2\pi. \tag{58}$$

For $B>1$, this is an unstable eigenfunction of the linearized problem, and is also an exact (stable) steady state for $B=1$. For $B<1$, simulations from this data show only decay to the

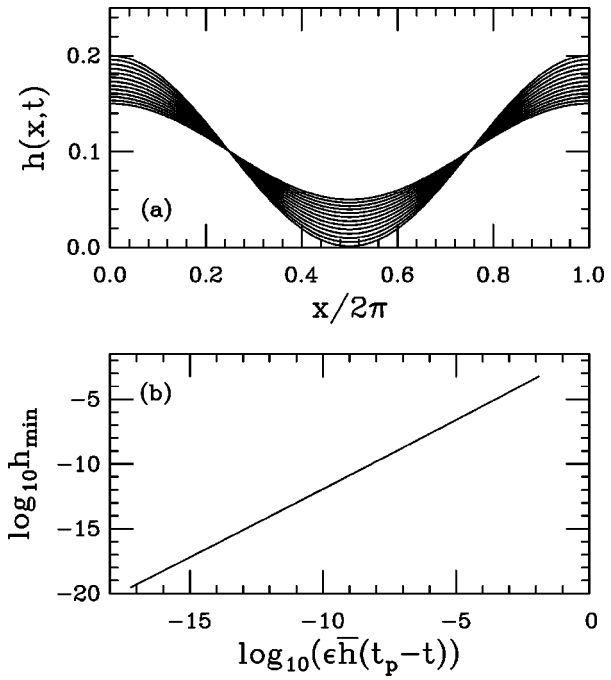

FIG. 4. (a) The slow evolution towards pinching for $B=1.05$. (b) The vanishing of the minimum thickness on a log–log scale.

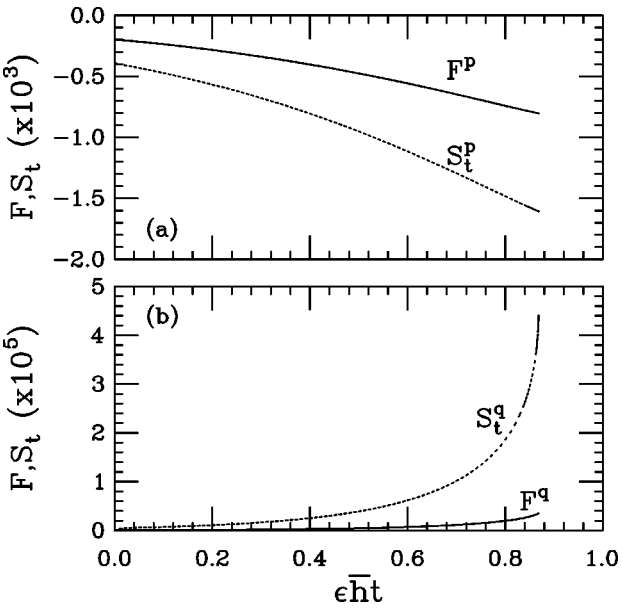

FIG. 5. Time evolution of energy F and entropy derivative S_t. (a) Contribution of the lower modes p. (b) Contribution of the higher modes q.

mean $\bar{h}$, as expected from linear theory. We note that Almgren *et al.*[12] have found special initial data which for $B=0$ show the formation of pinching singularities.

We consider here in greatest detail the case B slightly greater than unity, where the singularity occurs through a single, symmetric touchdown, and which allows comparison with a nonlinear theory developed in Sec. V. As B is increased, allowing more unstable length scales, there is an eventual ''splitting'' of this single singularity into two, as well as an apparent change in its type.

1. $B=1+\epsilon$, $\epsilon \ll 1$

When $B=1+\epsilon$, linear theory gives for the initial condition (58) a growth rate $\bar{h}\epsilon$. Data will typically be plotted relative to this (long) time scale. When $\epsilon \ll 1$ only the $k=1$ mode is unstable, while all higher modes are damped (the $k=2$ mode becomes linearly unstable only for $B \geqslant 4$). Figure 4(a) shows the evolution of h for $B=1.05$, with $\bar{h}=0.1$ and $a=0.5$. (h can be scaled out of the equation, but we did not do so.) This simulation uses adaptive time stepping and gridding, and quadruple precision, allowing us to follow $h_{\min}$ to very small levels. The simulations indicate that $h(x,t)$ reaches zero at the single point $x=\pi$, at the finite time $t_p \approx 173.7$. To demonstrate this, Fig. 4(b) shows $h_{\min}$ on a log–log scale, relative to an estimated pinch time t_p (see below), over many decades of decrease in $h_{\min}$. The curve is very close to being of unit slope, a point to which we will return.

A central point to much of what follows is the observation that as the minimum slowly descends h retains very closely a cosinusoidal shape. This is consistent with the linear analysis around the flat equilibrium, as noted above, and also with the PDE system being in proximity to the $B=1$ case, for which initial data (58) is a stable steady state for any a. Despite the oncoming singularity associated with the collapse, this observed separation of scales—the $k=1$ mode being active with higher modes remaining damped—is maintained surprisingly well.

To examine this, consider the two integral quantities associated with this system that decompose naturally in Fourier space—the energy $\mathscr{F}$ and the entropy time derivative $\mathscr{S}_t$. Both are quadratic and so are expressible as sums of squared amplitudes. Only $\mathscr{F}$ has a prescribed behavior; it must monotonically decrease. $\mathscr{S}_t$ is examined also because of its modal separability, though from the simulation for $B=1.05$, $\mathscr{S}$ itself decreases monotonically (i.e., motion away from the mean). If $h=p+q$, where p is the Fourier projection of h onto the m lower modes, and q the remainder, then the energy $\mathscr{F}$ divides naturally as

$$\mathscr{F}_p+\mathscr{F}_q=2\pi\sum_{|k|\leqslant m}\rho_k|\hat{h}_k|^2+2\pi\sum_{|k|>m}\rho_k|\hat{h}_k|^2, \qquad (59)$$

where $\rho_k=k^2-B$ and a conserved part due to the mean of h has been dropped. One has a like expression for $\mathscr{S}_t=\mathscr{S}_t^p+\mathscr{S}_t^q$. Figure 5(a) shows $\mathscr{F}^p$ (solid) and $\bar{h}\mathscr{S}_t^p$ (dashed), while Fig. 5(b) shows $\mathscr{F}^q$ and $\bar{h}\mathscr{S}_t^q$ for $B=1.05$. Choosing $m=1$ gives definite signs to the separate elements of the decomposition ($\rho_1<0$, $\rho_k>0$ for $k>1$). For the energy $\mathscr{F}$, $\mathscr{F}^p$, and $\mathscr{F}^q$ remain separated by three orders of magnitude, even as the singularity is approached.

Is mode damping responsible for keeping $\mathscr{F}^q$ small? To study this further, we examine the relative importance of the time derivatives p_t and q_t of the decomposed function h_t. If q_t is small relative to p_t, then the dynamics of the modes in q are slaved to those in p. For $\epsilon=0.05$, 0.1, and 0.2, Fig. 6(a) shows the ratio $|q_t/p_t|$ using $m=1$, at $x=\pi$. The singularity time—shown as a dashed line and decreasing with ϵ—is at the point where q_t reaches its greatest amplitude. We see three distinct behaviors. First, for a short initial time interval,

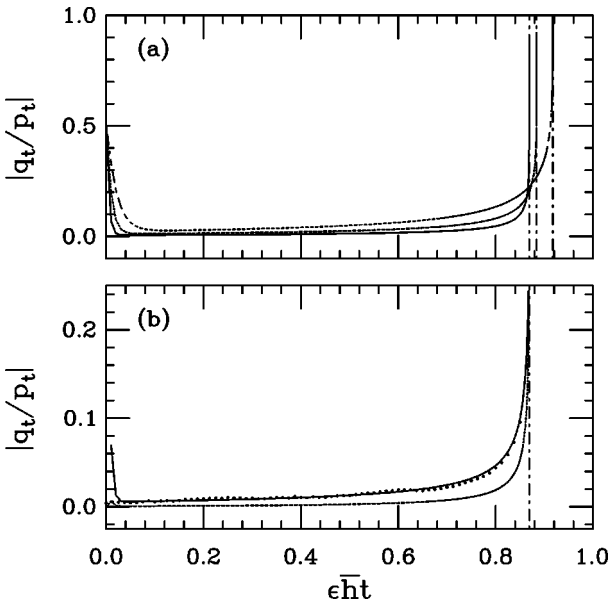

FIG. 6. Plots of the relative magnitudes of time derivatives of upper and lower modes. (a) Ratios as functions of (rescaled) time for $B=1.05,1.10,1.20$. Dashed lines are estimated pinching times (decreasing with ϵ). (b) Comparison of the ratio for $B=1.05$ for $m=1$ (upper solid curve) and $m=2$ (lower solid curve).

whose length decreases with ϵ, p_t, and q_t are of the same order and the ratio quickly relaxes to much smaller values. That these quantities must initially be of the same order follows simply from initial mode mixing in the quadratic nonlinearity. Second, until close to the singularity time, the ratio maintains a small value, with amplitude that decreases with ϵ. And third, near the singularity time, p_t and q_t become of the same order (although oppositely signed), though again the length of the time interval over which this is true decreases with ϵ. Lastly, inspection of q_t shows that the spatial extent around $x=\pi$ over which it is comparable to p_t decreases with ϵ.

Figure 6(b) compares the ratios $|q_t/p_t|$ for $m=1$ and 2, with $\epsilon=0.05$. For $m=2$, the initial relaxation period is removed, the ratio is smaller overall, and remains small until yet closer to the singularity time. In summary, it appears that over the the bulk of the evolution of the PDE, until very near the singularity time, the modes of q are slaved to those of p.

Separation of scales and slaving underlie an approximate ''slaving theory,'' developed in detail in Sec. V. However, to assist in the further interpretation of our numerical simulations, it is useful here to outline several of the theory's results.

In the simplest case, (setting $\bar{h}=1$) we decompose h as

$$h(x,t)=1+a(t)\cos x+q(x,t)=p+q,$$

i.e., $m=1$. By assuming that q is small and slaved to p, that is $q_t\approx 0$, q can be found as a functional of p and the amplitude $a(t)$ determined. Such a single mode representation for p is only accurate for $\epsilon\ll 1$, as suggested by Fig. 6. From these approximations we find that:

(1) $a(t)\to 1$ at a finite time t_p. This corresponds to a pinch in our slaving theory, and we find that near the singularity time $p_{\min}(t)\sim(t_p-t)+O((t_p-t)^{3/2})$.

(2) $q(x,t)$ has the Fourier series representation

$$q(x,t)=A(a)\sum_{k=2}^{\infty}(-1)^k\frac{e^{-\alpha(a)k}}{k^3-Bk}\cos kx, \tag{60}$$

which corresponds to a pair of complex pole singularities in the complex extension of q_{xxx}, located at $x=\pi\pm i\alpha$. As $t\to t_p$, $\alpha\to 0$, and analyticity of q is lost as the poles collide on the real axis at $x=\pi$.

(3) A local scaling form can be found for q_{xx} and q_{xxx} as $t\to t_p$

$$q_{xx}\sim\ln\sqrt{t_p-t}+\ln\left(1+\frac{1}{2}\eta^2\right)$$

$$q_{xxx}\sim-\frac{1}{\sqrt{t_p-t}}\left[\frac{1}{\eta-\sqrt{2}i}+\frac{1}{\eta+\sqrt{2}i}\right], \tag{61}$$

where $\eta=\text{Const}\cdot(x-\pi)/\sqrt{t_p-t}$.

True to its derivation, we do find that the slaving theory describes very well the approach of the system to the singularity, at which point its underlying assumptions break down (i.e., q_t becomes comparable to p_t), and some divergences are observed. However, using a change of scaling variable η very near the singularity time, as suggested by Almgren *et al.*,[12] we find that Eq. (61) do predict the apparent spatial form of the singularity. We turn back now to the results of the numerical simulations.

Again, much of the behavior of the PDE for $B=1+\epsilon$ can be collapsed by considering motion on the normalized time $t'=\epsilon\bar{h}t$. Figure 7(a) shows $h_{\min}$ (the solid curves) for several values of ϵ, with h evolved from the same initial condition as above. The solid curve closest to the dashed curve is that for $B=1.05$. The dashed curve arises from the slaving theory discussed in Sec. V; it is clearly the limiting behavior as $\epsilon\downarrow 0$.

We have fit the collapsing width with the Ansatz

$$h_{\min}(t')\sim(t_p'-t')^{\psi}, \tag{62}$$

using a nonlinear least-squares method over a sliding set of ten data points. Figure 7(b) shows t_p' as a function of ϵ. This figure shows the singularity times to deviate linearly in ϵ from a limiting value, determined by the slaving theory. Figure 7(c) shows the result of sliding fits to ψ, for several values of ϵ, as the singularity time is approached. The nonlinear theory gives that $h_{\min}(t')\sim(t_p'-t')+O((t_p'-t')^{3/2})$, and we include its fit, even though the form is known, as a check on the fitting procedure; the influence of the higher-order correction term is clear, though the ultimate convergence of ψ to unity is also apparent. Somewhat similar behavior is seen for finite values of ϵ. For times away from t_p, for each ϵ, the fit ψ is more or less constant, with value varying almost linearly in ϵ from unity. But very close to the singularity, the fit value for ψ begins a rapid decrease, perhaps to one.

Rather than examining the precise details of the singularity form, we first discuss an analytic structure of $h(x,t)$

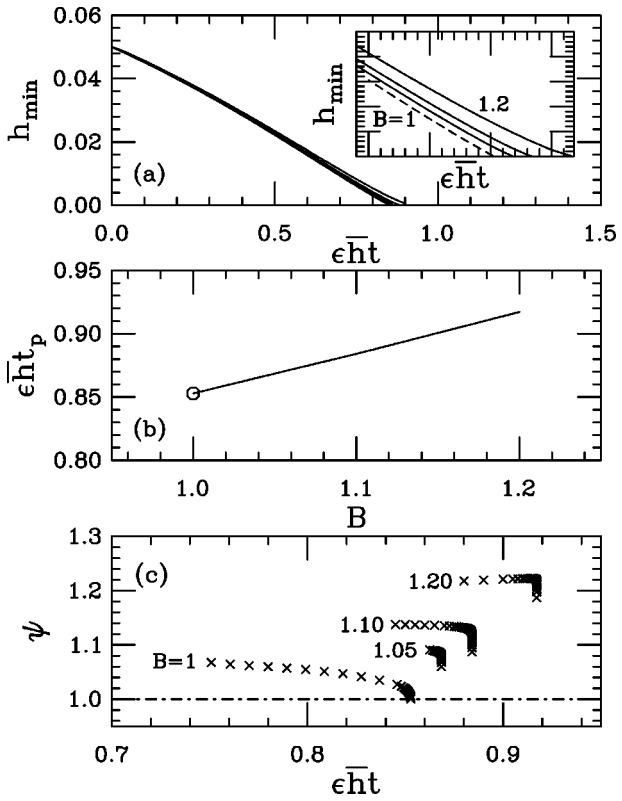

FIG. 7. Properties of the singularity. (a) The minimum of h, for several values of B, as a function of rescaled time. Inset: Close-up of behavior near pinch time. (b) Rescaled pinch time as a function of bond number. (c) Effective exponent near the pinch point as a function of time.

that emerges at early times and persists until quite close to the singularity. To do this, we study the Fourier spectrum $\hat{h}_k$. Figure 8 shows $\log_{10}|\hat{h}_k|$ for $B=1.05$ for times near the singularity time. This simulation was performed on a uniform mesh, again in quadruple precision (29 digits), rather than double precision (15 digits), to provide more of the decaying range of the spectrum for data fitting (see also Ref. 31).

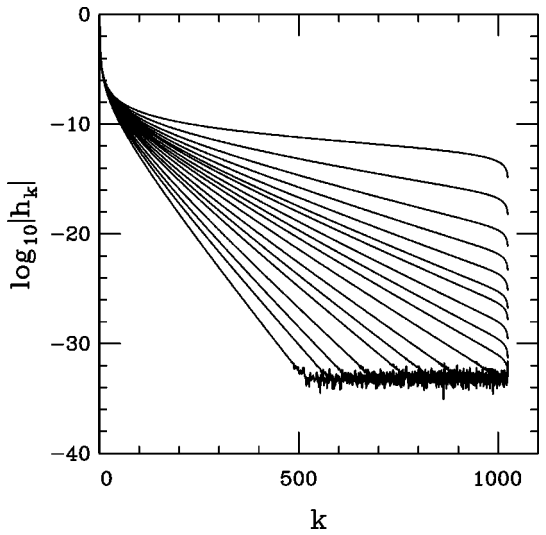

FIG. 8. Fourier spectrum of h as a function of time. Increasing time corresponds to decreasing decay.

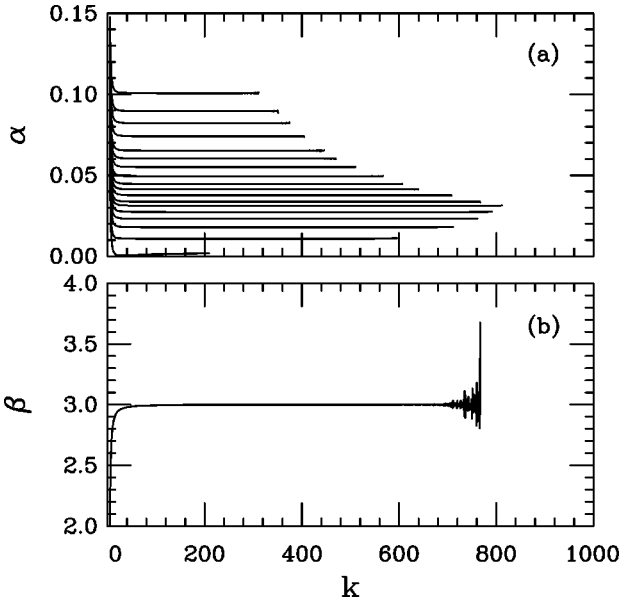

FIG. 9. Coefficients of the spectrum of h in Eq. (63). (a) The effective decay constant as a function of wave number and time. (b) The effective power-law exponent as a function of wave number very near the pinch time.

The approaching loss of smoothness in h is evidenced by a loss of decay in $\hat{h}_k$ (for $k \gg 1$) as the singularity time is approached. If the oncoming singularity is algebraic and isolated, then we anticipate that the large k behavior of the Fourier spectrum can be interpreted as that induced by two algebraic singularities, one above and one below the real axis

$$|\hat{h}_k(k,t)| \approx C(t) k^{-\beta(t)} e^{-\alpha(t)k} \tag{63}$$

(see also Refs. 28, 31, and 32). These singularities would be of order $\beta+1$, and lie a distance α above and below the x axis (i.e., α is the analyticity strip width). In this Ansatz, the singularity is signaled by α becoming zero at some time, and exponential decay in the spectrum being lost. The algebraic order of the singularity is then revealed by β. Using the approach in Shelley[31] (see also Sulem, Sulem, and Frisch[33]), we have fit values to C, β, and α, using a sliding fit to successive quadruplets (in k) of $|\hat{h}_k|$.

Figure 9 shows these fits at the times of the previous figure. The upper graph is that for α. The uppermost curve is the earliest time shown, and is the fit for the leftmost graph in Fig. 8. That the curves show irregular spacing reflects the use of adaptive time stepping in the numerical code. The fits are very flat in k, as desired, becoming noisier as decaying amplitudes approach the round-off level (at earlier times). As time proceeds, the amplitude at the Nyquist frequency rises above the round-off level, and the domain in k over which α achieves a flat fit decreases as truncation errors become important. At the last time shown, very close to the singularity time, the fit is hardly satisfactory. This also reflects the expectation that the calculation should become inaccurate as the analyticity strip width of the solution approaches the mesh spacing. And indeed, at the next-to-last time shown, the fit to α is ~ 0.011, while the mesh spacing itself is $2\pi/2048 \approx 0.006$.

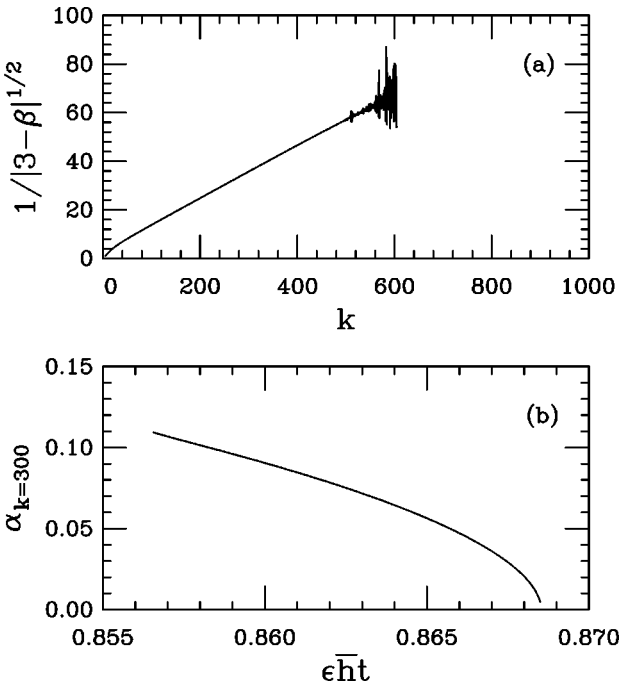

FIG. 10. Spectral coefficients. (a) The deviation of the power-law exponent from three. (b) Loss of the exponential decay.

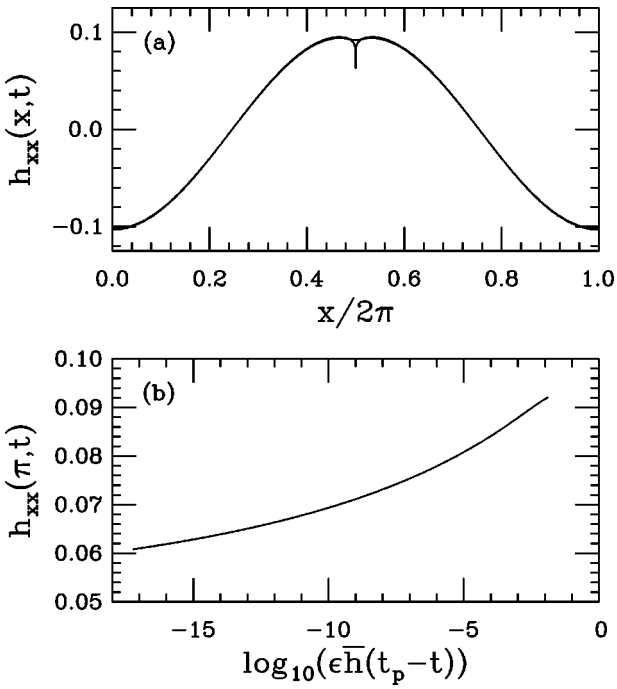

FIG. 11. (a) h_{xx} at several times as the singularity time is approached. (b) h_{xx} at $x=\pi$ on a logarithmic time scale, relative to the estimated singularity time.

The fits to β are represented by the one shown in the lower graph, which corresponds to the 12th time shown in the upper ($t' \approx 0.867$). On the region of β having a smooth fit, it appears very close to three. All the other times, in their respective regions of displaying a good fit, also lie close to three—this particular fit is shown because it has the broadest such domain in k. We note that because β governs the less dominant, algebraic part of the spectral decay, it is usually more difficult to determine well than α. Nonetheless, that β is very well fit by three is confirmed by Fig. 10, whose upper graph shows the discrepancy between three and the fit to β as a function of k. The difference seems to be decreasing as $1/k^2$ for $k \gg 1$. The lower graph of Fig. 10 shows α at the representative value $k=300$ as a function of time. It shows clearly the oncoming loss of smoothness. The singularity time predicted by α becoming zero corresponds closely to that of $h_{\min}(t)$. And so, examination of the spectrum from the uniform grid simulations suggests that its large k behavior is given by

$$\hat{h}_k \sim A(t)(-1)^k \frac{e^{-\alpha(t)k}}{k^3}, \tag{64}$$

in good agreement with the slaving theory. While we have been focusing on the behavior of the spectrum of h very near the singularity time, we emphasize again that this emerges at early times in the evolution.

If this precise spectral behavior were maintained to the singularity time, then in physical space there would occur a logarithmic spatial singularity in h_{xx}, with $h_{xx} \downarrow -\infty$ logarithmically in time, as in Eq. (61). However, as A. Bertozzi[34] has pointed out, h_{xx} becoming negative at $x=\pi$ is inconsistent with having a single minimum of h as the singularity time is approached. In light of this we examine our adaptive simulations.

Figure 11(a) shows $h_{xx}(x,t)$ at several times near the singularity time, which is seen to be developing a very sharp structure around $x=\pi$, while Fig. 11(b) shows $h_{xx}(\pi,t)$ on a logarithmic time scale, again relative to t_p. While $h_{xx}(\pi,t)$ is decreasing, it is doing so very slowly, and is certainly not becoming negative on the range of scales to which we have been able to compute. Moreover, this graph has a persistent upward curvature which is not consistent with a logarithmic divergence, as predicted by Eq. (61), and may instead be showing saturation to a finite value as t_p is approached.

This discrepancy from the slaving theory is reinforced by Fig. 12(a), which shows h_{xxx} in rescaled coordinates as the singularity time is approached. We have plotted $\sigma h_{xxx}(\eta,t)$, where $\eta=(x-\pi)/\sigma$ and $\sigma=A(t_p-t)^{1/2}$, where A is a constant. This rescaling does only a fair job of collapsing the behavior of h_{xxx} as it varies over five orders of magnitude, but suggests that h_{xxx} is diverging as something close to an inverse square-root behavior. This rescaling was motivated by Fig. 12(b), which shows the the divergence of $\max |h_{xxx}|$, on a log–log scale (relative to t_p). On this scale, the curve is quite flat with a slope very close to $-\frac{1}{2}$.

A far superior rescaling of the data is found by following the suggestion of Almgren, Bertozzi, and Brenner[12] in their study of symmetric singularity formation in the unforced case ($B=0$), namely to collapse the data very near the singularity time on the intrinsic length scale $\zeta = [h(\pi,t)/h_{xx}(\pi,t)]^{1/2}$. As an Ansatz we consider the scaling functions suggested by the slaving theory, Eq. (61)

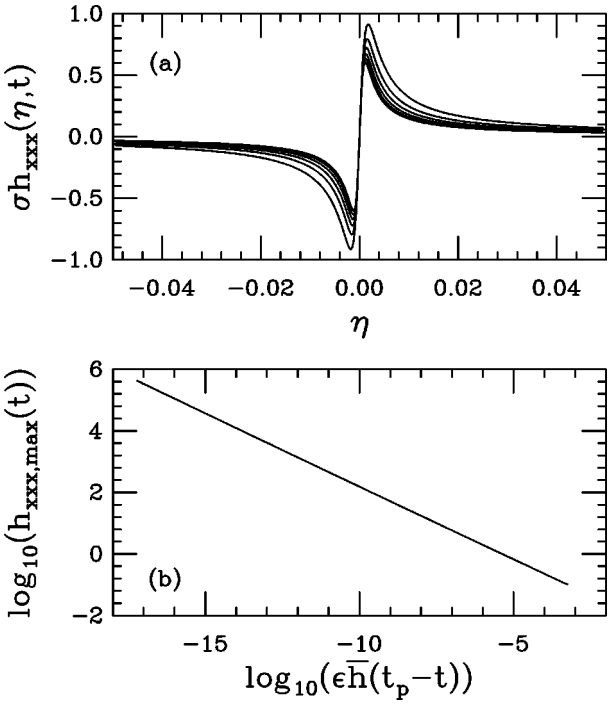

FIG. 12. (a) h_{xxx} in rescaled coordinates as the singularity time is approached. See text for details. (b) The divergence of max $|h_{xxx}|$ on a log–log scale, relative to the estimated singularity time.

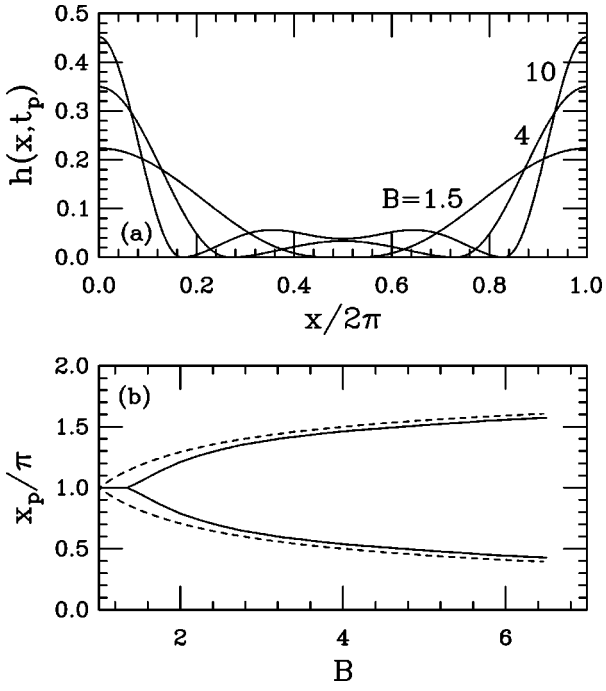

FIG. 14. Singularity splitting. (a) Interfaces near touchdown for various bond numbers. (b) Bifurcation of the touchdown points (solid) compared with asymptotic form (dashed).

$$h_{xx}\sim C+D\,\ln(1+\tfrac{1}{2}\eta^2),\quad h_{xxx}\sim\frac{D}{\zeta}\,\frac{\eta}{1+\tfrac{1}{2}\,\eta^2},\qquad(65)$$

with $\eta=(x-\pi)/\zeta$. C and D are then determined as

$$C=h_{xx}(\pi,t)\quad\text{and}\quad D=\zeta^2 h_{xxxx}(\pi,t).$$

To lay bare this presumed scaling in the numerical solution, we plot $(h_{xx}-C)/D$ and $\zeta h_{xxx}/D$, as functions of η and t, in Figs. 13(a) and 13(b), respectively. At earlier times, we see the emergence of scaling behavior at $\eta=0$, with both functions converging to a single form. These forms do indeed seem to be given by the scaling functions $\ln(1+\eta^2/2)$ and $\eta/(1+\eta^2/2)$, also plotted in Figs. 13(a) and 13(b), respectively, as dashed curves but obscured by the converging graphs.

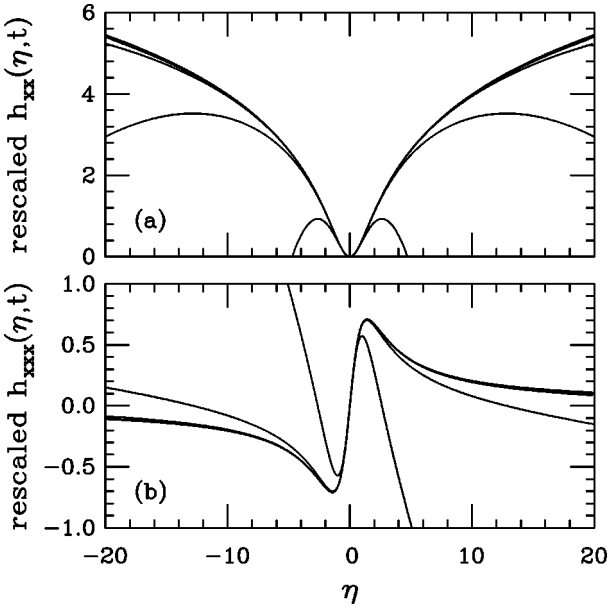

FIG. 13. Results of rescaling on an intrinsic length.

And so the slaving theory appears to predict the spatial forms of the singularity, though there are departures in terms of the inner scaling and temporal behavior. This is also the same singularity structure uncovered by Almgren *et al.*[12] in their study of symmetric singularities in the unforced case, and they also give numerical evidence for the emergence of a larger, second length scale around the singularity region. If interpreted in the language of complex singularities, this suggests the development of a singularity structure more complicated than, say, a single pair of poles in h_{xxx}, though that form does apparently govern the innermost scale.

C. As *B* increases

The number of unstable length scales in the 2π period increases as $\sqrt{B}$ with increasing B. This increase in the number of unstable scales leads eventually to a splitting of the singularity for B sufficiently large, i.e., for $B\approx 1.35$. The upper graph of Fig. 14 shows $h(x,t)$ near pinching for $B=1.5$, 4.0, and 10, respectively. As B increases, the distance between the bifurcated singularities increases, leaving trapped regions of fluid between the ''Rayleigh–Taylor'' spikes about $x=0$ and 2π. The lower graph shows the location of the two critical points as a function of B (the solid curves). The dashed curves are $(B,\pi/\sqrt{B})$ and $(B,\pi(2-1/\sqrt{B}))$. These curves correspond to a spike width of $2\pi/\sqrt{B}$, the most unstable length scale, as well as give the width of the weak solution (26), given in Sec. III A. For

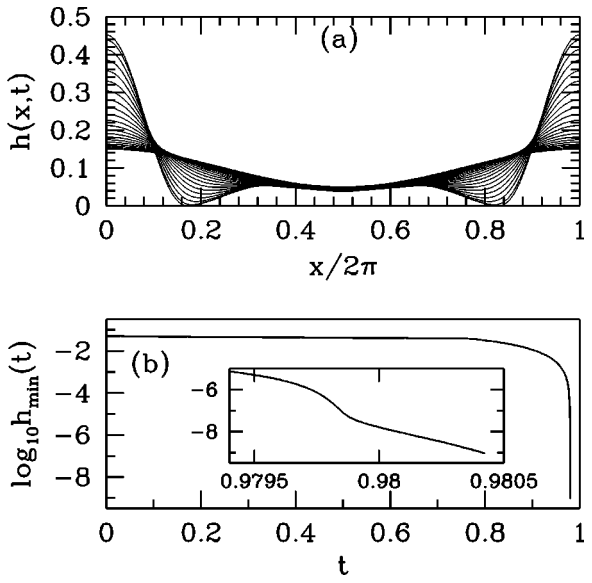

FIG. 15. The functions $h(x,t)$ (a) and $h_{\min}(t)$ (b) as pinching in the system is approached. Inset in (b) shows detail of $h_{\min}$ near the end of the simulation.

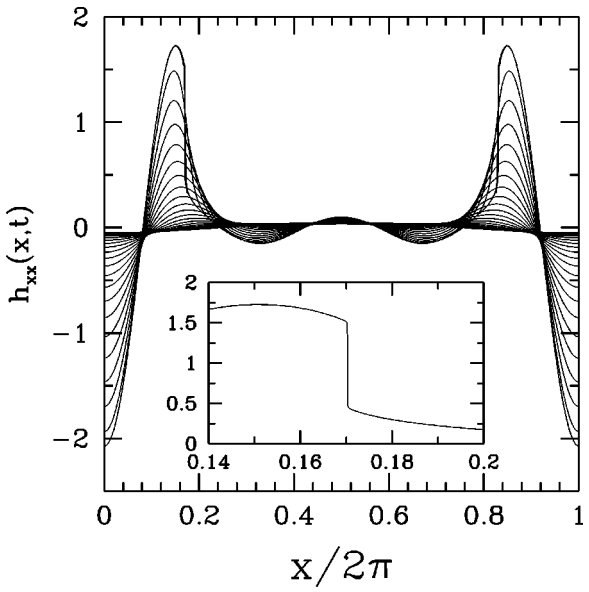

FIG. 16. $h_{xx}(x,t)$ as pinching in the system is approached. Inset shows detail of jump discontinuity in the pinch region.

larger B, this length not only describes the width of the observed spikes, but the weak solution with properly chosen amplitude also fits closely the spatial form of the spike.

We concentrate on the $B=10$ case, for which the most unstable wave number is $k^*\approx 2.2$. Figure 15(a) shows $h(x,t)$ at several times, as the lubrication approximation is evolved from the initial condition (58). Again, an approach to pinching is observed, and as remarked previously $h(x,t)$ pinches asymmetrically, in contrast to the symmetric pinching observed for values of B near one. Figure 15(b) shows $\log_{10} h_{\min}(t)$. In the initial stages of the collapse, $h_{\min}$ is given by $h(\pi,t)$ as the unstable $k=1$ mode grows in amplitude. However, nonlinearity feeds energy into the smaller scales, including those near that which is most unstable, and new minima appear at the sides of the developing spikes.

Figure 16 shows h_{xx}, with the inset showing the details in the pinch region. In further contrast to the behavior for B near one, now h_{xx} appears to develop a jump discontinuity, with an accompanying divergence in h_{xxx}. This ultimate jump discontinuity in h_{xx} would suggest again [as in Eq. (64)] a large k behavior governed by a cubic algebraic decay multiplied by an exponential decay that is being lost. In such a form, it is anticipated that the approach to the real x axis of two simultaneous, oncoming singularities in h will produce an additional oscillation in k of wavelength $2\pi/x_p$. This is consistent with the observed behavior in Fig. 17, which shows $\log_{10}|k^3\hat{h}_k|$ (from a uniform mesh simulation) versus k, as the singularity is approached. While we have not tried to fit this behavior, on a logarithmic scale it shows the anticipated linear decrease, overlaid by an oscillation of the expected wavelength.

Again, if this spectral behavior persisted, it would indicate the ultimate collision on the real axis of pole singularities in the analytic extension of h_{xxx}. We consider again our adaptive simulations in the neighborhood of the incipient singularity, again rescaling the data on the variable $\eta=(x-x_{\min})/\sigma$, $\sigma=[h(x_{\min},t)/h_{xx}(x_{\min},t)]^{1/2}$. We find that in this rescaled variable that h_{xxx} is very nearly an even function, suggesting that in terms of poles

$$h_{xxx}\sim \frac{A}{1+\frac{1}{2}\eta^2}=\frac{A}{\sqrt{2}i}\left(\frac{1}{\eta-\sqrt{2}i}-\frac{1}{\eta+\sqrt{2}i}\right),$$

where $A=h_{xxx}(x_{\min},t)$. In Figs. 18(a) and 18(b) we plot the even and odd parts of $h_{xxx}(\eta,t)/A$. In Fig. 18(a) is also plotted, as a dashed curve, the scaling form $1/(1+\eta^2/2)$, again obscured by the relaxation of other curves to it. We see in the odd part [Fig. 18(b)] the appearance of a persistent correction (at about 3%) to the apparent (even) pole structure. At early times in the figure, the odd part has the appearance of the pole arrangement seen for the symmetric singu-

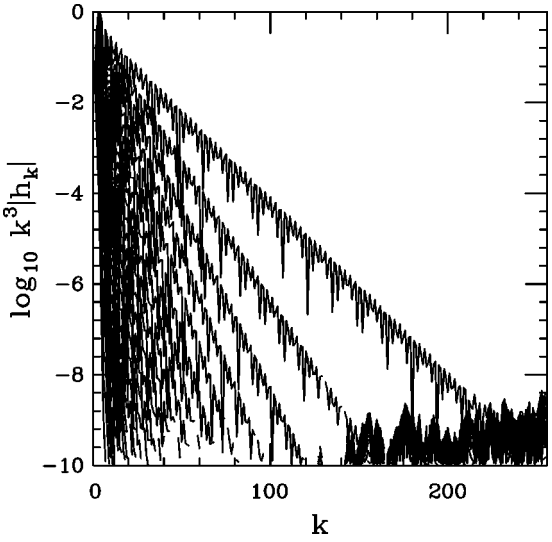

FIG. 17. Spectrum of h, multiplied by k^3, corresponding to evolution in Fig. 16.

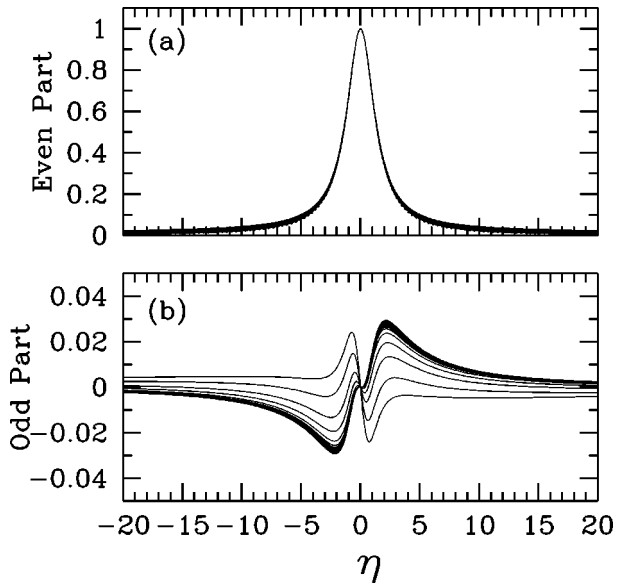

FIG. 18. The decomposition of $h_{xxx}(\eta,t)/A$ into even (a) and odd (b) parts, as a function of η.

larity structure at smaller bond numbers, but it develops into a more complicated form as the singularity develops.

For these simulations, we have skirted the issue of whether $h_{\min}\downarrow 0$ at a finite time. Up to about $t\approx 0.9798$ ($h_{\min}\approx 2\times 10^{-7}$) $h_{\min}$ shows a rate of decrease that if maintained would yield a finite time pinch. However, at this time, there is an abrupt slowing of $h_{\min}$ in its descent. This is shown in the inset of Fig. 15(b), showing this slowing on a log scale in h. It is also at this slowing time that there is a transition in the odd part of $h_{xxx}(\eta,t)$ (see Fig. 18) from what looks like the odd two pole arrangement of Eq. (65), to some more complicated structure.

In the unforced ($B=0$) case Almgren *et al.*[12] also studied ''exploding'' singularities, in which two singularities emerge from what is initially a single minimum, and which may describe the double singularity that appears in the splitting near the bifurcation point in Fig. 14. Such singularities were studied and quantified earlier by Dupont *et al.*[9] for the $B=0$ equation being forced by boundary conditions. In their analyses of this singularity, both studies predict a behavior of $h_{\min}\sim((t_p-t)/\ln(t_p-t))^2$. However, the descent here is slower, showing a nearly linear decrease on the log scale. Of course, from our spectral simulations we have less than two decades of decrease in this regime. Though not shown here, less accurate finite-difference simulations (these are considerably faster to perform) show an apparent continuation of this behavior. In some agreement with these studies, we do observe at this transition a ''slowing down'' in the motion of x_p, though it is unclear if the post-transition behavior will be to a constant velocity, as predicted in Refs. 9 and 12. We do not yet know if the behavior found in these other studies is universal, and applies here. Indeed, another possibility is infinite time relaxation, without intervening singularity, to an asymptotic state incorporating a weak solution (see Sec. III A). Such a situation was studied by Constantin *et al.*[8] for a $B=0$ case, again being forced by boundary conditions. We do note that a two-mode slaving approximation (discussed in the next section), which may serve to describe an ''outer solution'' at least near the bifurcation (in B) to two touchdowns, does not show any transitions in behavior as touchdown is approached. There we find that x_p approaches the pinch with constant velocity, with $p_{\min}$ decreasing to zero linearly in time (as did the single mode case).

V. THE DYNAMICS OF SMALL-SCALE SLAVING

A. Partitioning of scales

We have seen in the previous section that the global aspects of the Rayleigh–Taylor instability in Hele–Shaw flow are primarily controlled by the Bond number. Beyond but still near the critical value $B=1$, a single unstable mode dominates the flow, leading to a symmetric touchdown at $x=\pi$. Even at the singularity time the amplitudes of the higher Fourier modes remain small, although decaying only algebraically with mode number. Further increase in B leadsultimately to singularity splitting; two asymmetric touchdowns straddling $x=\pi$. This phenomenon is associated with the presence of an appreciable amplitude of the first harmonic ($\cos 2x$). Still, modes three and above remain small. Based on the linear stability analysis of the previous section, we see that when B is close to unity the growth rates of the higher modes are all negative and $\mathcal{O}(1)$, while that of the unstable $m=1$ mode is small. This suggests a separation of time scales like that used in the derivation of amplitude equations for convective and lasing instabilities.

These observations further suggest that one might construct an approximate dynamics based on the dominance of the active modes over the linearly stable small-scale modes. A natural approach is to partition h into low (p) and high (q) modes by means of an operator $\mathcal{P}_m$ that projects a periodic function onto its lower m modes, where the number m includes at least those that are linearly unstable. Thus we write

$$h=p+q \quad (\mathcal{P}_m p=p, \quad \mathcal{P}_m q=0), \tag{66}$$

and seek a reduced dynamics for the lower modes in terms of their time-dependent amplitudes.

A useful simplification in developing the slaved dynamics arises from the fact that the RHS of the Rayleigh–Taylor Eq. (9) may be integrated further, so that it has the form

$$h_t=-\partial_{xx}(hh_{xx}-\tfrac{1}{2}h_x^2+\tfrac{1}{2}Bh^2). \tag{67}$$

Now substituting the decomposition (66) into the lubrication PDE (67), we make the fundamental slaving hypotheses; (a) ignore contributions of order q^2, and (b) ignore the time dependence of the high modes ($q_t\simeq 0$). We obtain the linear inhomogeneous differential equation for the high modes q

$$pq_{xx}-p_xq_x+(p_{xx}+Bp)q=-\tilde{\tilde{p}}_t-\tilde{J}_p+C, \tag{68}$$

where $J_p=p\mathcal{L}_B p$ is the flux associated with the lower modes, C is an integration constant, and for any function $f(x)$ we define

$$\tilde{f}=\int^x dx' f(x'). \tag{69}$$

By construction, the function p is periodic in x, and thus Eq. (68) is the inhomogeneous Hill equation,[35] in which both the function q and the time dependence of the lower modes, $\tilde{\bar{p}}_t$, are unknowns.

Equation (68) may be cast in the more standard form of Hill's equation by the transformation

$$q(x)=\sqrt{p(x)}\mathcal{Q}(x), \tag{70}$$

where $\mathcal{Q}$ obeys

$$\left(\frac{d^2}{dx^2}+B+3\,\frac{2pp_{xx}-p_x^2}{4p^2}\right)\mathcal{Q}=\frac{\tilde{\bar{p}}_t+\tilde{J}_p-C}{p^{3/2}}. \tag{71}$$

The explicit appearance of the factor of B inside the operator in (71) makes it clear that the natural periodicity of the system, at least for small deviations from a planar state, is $\sqrt{B}$, incommensurate with that of the lower modes when $B\neq 1$. This representation has the disadvantage that the clear separation of modes in the initial partition (66) has been lost in the transformation (70).

1. Spectral properties of q

To illustrate the means by which Eq. (68) is solved both for q and $\tilde{\bar{p}}_t$, consider the simplest hypothesis for the active modes

$$p=1+a(t)\cos x. \tag{72}$$

In light of the linear stability result $a_t=\overline{h}(B-1)a$ and the similar scaling of the flux J_p with $(B-1)$, a natural set of rescalings to adopt is

$$\tau=(B-1)\overline{h}t; \quad q=(B-1)Q, \tag{73}$$

reducing (68) to an inhomogeneous form of Ince's equation[35]

$$(1+a\,\cos x)Q_{xx}+a\,\sin xQ_x+[B+(B-1)a\,\cos x]Q$$
$$=(a_\tau-a)\cos x-\frac{a^2}{4}\cos 2x, \tag{74}$$

where we have determined the integration constant in Eq. (68) to be $C=(1+a^2/2)/2$ in order that the RHS of (74) have zero mean value.

Now we turn to the solution of the inhomogeneous Ince Eq. (74) for general values of the bond number. It is an alternating Fourier series of the form

$$q=\sum_{n=2}^{\infty}(-1)^nC_n\cos nx. \tag{75}$$

Direct substitution into Eq. (74) yields the relations for the first two modes

$$C_2=\frac{2}{a(B-7)}(a_\tau-a),$$

$$C_3=\frac{2}{a(B-13)}\left[\frac{a^2}{4}+(B-4)C_2\right], \tag{76}$$

while for $n\geqslant 4$ the recursion relation is

$$\frac{a}{2}(n^2+3n+3-B)C_{n+1}-(n^2-B)C_n$$
$$+\frac{a}{2}(n^2-3n+3-B)C_{n-1}=0. \tag{77}$$

A first observation concerns the asymptotic behavior of the C_n's for $n\gg 1$, which may be deduced using standard methods for difference equations.[36] In brief, for $n\to\infty$ the recursion relation (77) simplifies to

$$\frac{a}{2}C_{n+1}-C_n+\frac{a}{2}C_{n-1}=0, \tag{78}$$

for which one readily verifies the exponential behavior

$$C_n\sim\lambda^n, \tag{79}$$

where λ satisfies the quadratic equation

$$a\lambda^2-2\lambda+a=0, \quad \lambda_\pm=\frac{1}{a}[1\pm\sqrt{1-a^2}]. \tag{80}$$

Note that $\lambda_+\lambda_-=1$, and in general, $\lambda_+\geqslant 1$ and $\lambda_-\leqslant 1$. The equality holding only when $a=1$, which corresponds to a touchdown of the lower modes.

More information on the large-n behavior is obtained by writing $C_n=\lambda^nD_n$ and using the same methods, whereby one finds $D_n\sim n^{-3}$ independent of B. We thus conclude that for large n the solution to the recursion relation has the form

$$C_n\sim\sum_{\nu=\pm}A_\nu\frac{\lambda_\nu^n}{n^3} \quad (n\gg 1). \tag{81}$$

Clearly the solution corresponding to λ_+ does not satisfy the requirement of boundedness. The solvability condition is that the solution be bounded, which now means that a_τ, the only unknown in the recursion relations (76), should be chosen such that $A_+=0$. We have not succeeded in finding a closed form analytic solution for $a(\tau)$ for general B, although one can be found in the special limit $B\to 1$ (see below). Nevertheless, a_τ as a function of a, and thence $a(\tau)$, may be found through a very straightforward numerical procedure described below.

The goal of the numerical procedure is to find a_τ, for given B and a, such that the growing solution given by the recursion relation is eliminated. Note the crucial feature that with B and a fixed, A_+ is a linear function of a_τ since the only place in the recursion in which a_τ occurs explicitly is in the amplitude C_2. Thus, an arbitrary guess for a_τ can be used to find the exact value by means of a Newton–Raphson method that will converge in a single step.

Figure 19(a) shows the function $a_\tau(a)$ so obtained for several different values of the Bond number. Even for B quite far from unity the general features of the function remain unchanged. In particular, all of the curves asymptote to the same linear behavior $a_\tau=a$ as $a\to 0$, simply reflecting the analytic linear stability result. Moreover, all converge to $\frac{1}{2}$ from above as $a\to 1$. Finally, note that the larger is B, the lower is the curve $a_\tau(a)$. This implies a delay in the rescaled pinch time that grows larger with B.

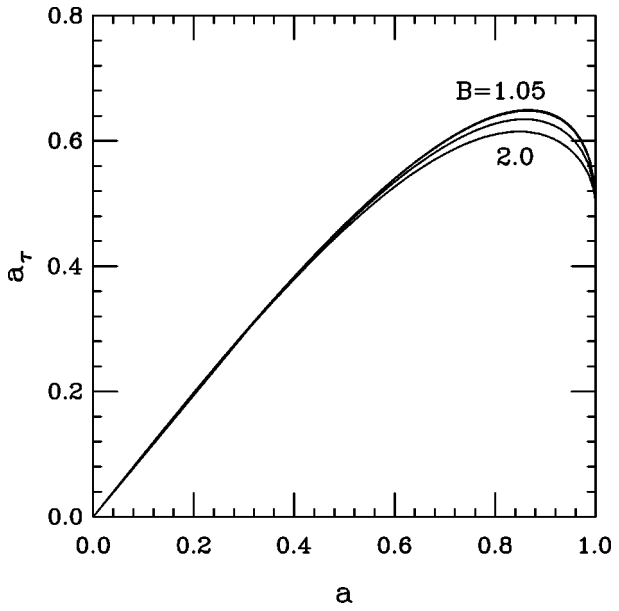

FIG. 19. Curves corresponding to the solvability condition for bond numbers 1.05, 1.5, and 2.0.

It can be shown that any Ansatz for the active modes contained in p generates a set of zeros in the complex plane, and the asymptotic spectrum is always of the form

$$C_n \sim \sum_{\nu=1}^{2m} A_\nu \frac{\lambda_\nu^n}{n^3} \quad (n \gg 1). \tag{82}$$

Elimination of the secular solutions associated with the m values of $\lambda > 1$ constitutes the m solvability conditions that determine the time evolution of the mode amplitudes. Some of these singularities will move toward, although not all reach the unit circle as the pinch time is approached.

2. An alternative slaving approximation

We now discuss an alternative version of the slaving approximation that makes use of these results on the spectrum of q. The difference of this new approach lies in the possibility of neglecting one other term that can be shown to be of higher order. A remarkable consequence of the irrelevance of that term will be a partial decoupling of the lower and higher modes, achieved through the definition of an auxiliary function.

We shall now proceed with the detailed explanation. By substitution of the spectral decomposition of $h(h=p+q)$ into the full equation of motion, Eq. (9), it becomes clear that for the large k limit there is a term $q\mathscr{L}p$ which is of even higher order than the temporal derivative q_t and thus that can be consistently neglected. These manipulations lead to a simpler slaving approximation, that can be summarized in the following set of equations:

$$p_t = -(p\mathscr{L}(p+q))_x, \quad \mathscr{P}_m p = p, \quad \mathscr{P}_m q = 0, \tag{83}$$

where $\mathscr{P}_m$ is the projection operator for the first m modes. Notice the very important feature that the shallow-water form persists after all the transformations and approximations.

It is possible to introduce still some further simplifications of this system. In fact, as p_t has zero mean, we define a new function y such that $y_x = p_t$. After replacing it in Eq. (83) and integrating once with respect to the variable x the slaving equation reduces to

$$\frac{y}{p} = -\mathscr{L}(p+q). \tag{84}$$

The lack of an arbitrary constant of integration is the consequence of $p\mathscr{L}p$ being a perfect derivative, and the orthogonality of the functions p and q. It is possible to decouple the evolution of p from q

Now we apply the projection operators $\mathscr{P}_m$ and $\mathscr{Q}_m$, where $\mathscr{P}_m$ is defined as before and $\mathscr{Q}_m$ is the operator that projects a periodic function onto its modes higher than m. The slaving approximation then becomes

$$p_t = y_x, \quad \mathscr{P}_m \frac{y}{p} = -\mathscr{L}p, \tag{85}$$

$$\mathscr{Q}_m \frac{y}{p} = -\mathscr{L}q. \tag{86}$$

In this description, the determination of the correction q is now completely decoupled from the evolution of p. The system of Eq. (85) is a natural, albeit nonstandard, Galerkin approximation to the lubrication equation, and one that retains the variational features of the original equation. Namely, the functionals $\mathscr{F}[p]$ and $\mathscr{S}[p]$, as defined in the previous section, are the energy and the entropy, respectively, and satisfy the same evolutions and inequalities (see Appendix C; also see Ref. 37 for dissipative Galerkin schemes for the Kuramoto–Sivashinsky equation).

The function p is the finite Fourier series

$$p(x,t) = \sum_{k=-m}^{m} a_k(t) e^{ikx}. \tag{87}$$

Since p is even and real, the coefficients a_k are real and satisfy $a_k = a_{-k}$. We now introduce the analytic continuation of the function p through the new variable $\theta = x + iv$. For convenience we use the notation $z = e_{i\theta}$. Therefore, Eq. (87) can be rewritten as

$$p(z,t) = \frac{1}{z^m} \sum_{k=-m}^{m} a_k z^{k+m} = \frac{1}{z^m} U(z), \tag{88}$$

where the function $U(z)$ is a polynomial of degree $2m$, and so has $2m$ zeros. Since the amplitudes a_k are real and symmetric, if λ is a complex zero of U, then its conjugate, λ^* and its inverse $1/\lambda$ will also be zeros of U. If $p > 0$ for $|z| = 1$, then U has no zeros on the unit circle. Then obviously m of the zeros lie within the unit circle, and m without. This allows us to rewrite $U(z)$ as the product

$$U(z) = A \prod_{k=1}^{m} (z - \lambda_k(t)) \left(z - \frac{1}{\lambda_k(t)} \right), \tag{89}$$

where $|\lambda_k| < 1$ and A and λ are functions of the amplitudes a_k.

Now we construct the function y from p, using (83). Since y has zero mean value, it can be written in the form

$$y(z,t)=i\,\frac{z^2-1}{z^m}\sum_{k=1}^{m}\tilde{U}_k(z)\dot{a}_k(t), \tag{90}$$

where $\tilde{U}_k$ is a polynomial of degree $2m-2$. The left hand side of (85) involves applying the projection operator $\mathscr{P}_m$ to the ratio y/p. This is simply a matter of finding $2m+1$ Fourier amplitudes. Using the properties of evenness and area conservation, the projection actually involves only m contour integrals for $k=-m,-m+1,...,-1$ of the form

$$\frac{1}{2\pi}\int_0^{2\pi}dx e^{-ikx}f(x)=\frac{1}{2\pi i}\int_{|z|=1}dz z^{-k-1}f(z). \tag{91}$$

When applied to $f=y/p$ these projections become the sum of residues at the zeros λ_k. Assuming that the λ_k's are all simple zeros, the system (85) can be calculated as the linear set of equations for $\dot{a}_k(t)$

$$\sum_{n=1}^{m}\left(\sum_{j=1}^{m}\frac{\lambda_j^k\tilde{U}_n(\lambda_j)}{\Pi_{\substack{p=1\\p\neq j}}^{m}(\lambda_j-\lambda_p)(\lambda_j-1/\lambda_p)}\right)\dot{a}_n(t)$$
$$=-A(a)(k^3-Bk)a_k. \tag{92}$$

Equation (92) constitutes a closed set of algebraic relations that completely determines the time evolution of the modes $a_k(t)$.

B. The dynamics of zeros

Once the values of all the λ_k's are obtained, every other related quantity can be determined, at least in an implicit fashion. Indeed, since the mean of p is conserved, the prefactor A can be given, in general, as a function of the λ_k's, which we represent as $A=A(\lambda)$, yielding in turn the a_k's. As a consequence of this, the system (85) can also be recast as the dynamics of the zeros of p by means of a residue calculation analogous to the previous one. The end result is

$$\sum_{n=1}^{m}\left(\sum_{j=1}^{m}\frac{\lambda_j^k\hat{U}_n(\lambda_j;\lambda)}{\Pi_{\substack{p=1\\p\neq j}}^{m}(\lambda_j-\lambda_p)(\lambda_j-1/\lambda_p)}\right)\dot{\lambda}_n(t)$$
$$=-A(\lambda)(k^3-Bk)a_k(\lambda), \tag{93}$$

where $\hat{U}_k(z;\lambda)$ is a polynomial of degree $2m-2$, with its coefficients being functions of the λ_k's.

1. Special cases for modal dynamics

$\underline{m=1}$: We choose $p=1+a\cos x$ and deduce from (92)

$$a_t=(B-1)\,\frac{a}{2}\,(1+\sqrt{1-a^2}). \tag{94}$$

This result can also be obtained analytically within the previous slaving approximation in the limit $B\to 1$.[7] It is found from Eq. (74) by setting $B=1+\epsilon$, rescaling t, and applying the solvability condition through the method of variation of parameters. For this purpose, we note that a general feature of the Ince Eq. (68) is that the Wronskian is equal to the lower mode function $p(x)$. A third approach, different from the two ''slaving'' approximations given here, is found in Appendix B. In this approach, p and q are found simply as successive terms in an asymptotic expansion of h in powers of ϵ.

In the rescaled time $\tau=(B-1)t$, Eq. (94) is solved as an implicit equation for $a(\tau)$, given the initial value $a_0\equiv a(\tau=0)$

$$f(a_0)-f(a)=\tau \tag{95}$$

where

$$f(a)=\frac{1-\sqrt{1-a^2}}{a^2}-\log\left(\frac{1-\sqrt{1-a^2}}{a}\right). \tag{96}$$

Pinching occurs when $a(\tau)\nearrow 1$ at the time

$$\tau_p=f(a_0)-1,\quad \text{or}\quad t_p=\frac{f(a_0)-1}{(B-1)}. \tag{97}$$

Let us note several important features of solutions (94)–(97). First, when the interface is nearly flat we obtain a weakly nonlinear equation of motion

$$a_\tau\simeq a-\frac{1}{4}a^3+\cdots,\quad (a\ll 1), \tag{98}$$

showing that the nonlinearities of the lubrication dynamics slow down the exponential growth $a(\tau)=a_0\exp(\tau)$ described by the linear stability analysis. Indeed, near the pinch time the amplitude is linear in time

$$a(\tau)\simeq 1-\tfrac{1}{2}(\tau_p-\tau)+\cdots,\quad (\tau\nearrow t_p). \tag{99}$$

A second issue concerns the scaling of the pinch time. When the initial amplitude is small, so that its initial growth is well described by exponential amplification, we find

$$t_p\sim\frac{\log(2/a_0)}{\overline{h}(B-1)}. \tag{100}$$

The logarithmic form of this behavior is what one would obtain by simply continuing the exponential growth until $a=1$, although the particular factor of 2 in (100) does not emerge from so simple an estimate.

Figure 20 shows excellent agreement between these asymptotic results and numerical studies of the lubrication PDE (9) for the pinch times $t_p(a_0)$, and for the minimum height $h_{\min}=(1-a(t))$.

The correction function q can now be obtained in closed form

$$q(x)=\lambda_+\left\{\sqrt{1-a^2}\,\sin x\,\tan^{-1}\left(\frac{\lambda_-\sin x}{1+\lambda_-\cos x}\right)\right.$$
$$+\frac{1}{2}(a+\cos x)\ln(1+2\lambda_-\cos x+\lambda_-^2)$$
$$\left.-a\left(\frac{3}{4}\lambda_-\cos x+\frac{1}{2}\right)\right\}. \tag{101}$$

Here $\lambda_\pm$ are the two real zeros of the quadratic previously introduced in Eq. (80). As $a\nearrow 1$, $\lambda_-\to 1$, and thus within this analysis the interface curvature, through $q''(x)$, develops a logarithmic singularity. This divergence can also be inter-

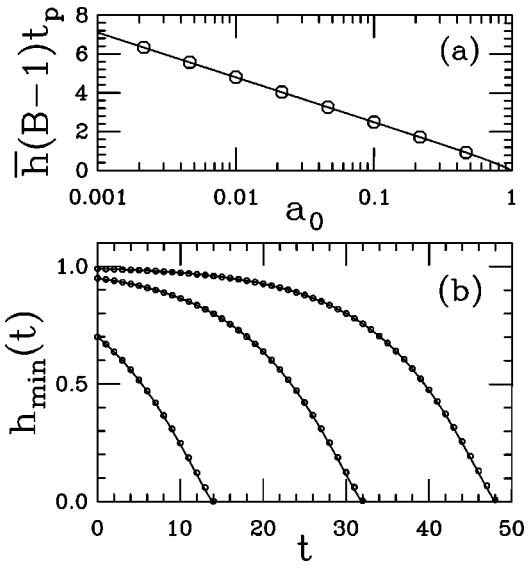

FIG. 20. Comparison between $B=1+\epsilon$ calculation and numerical results. (a) Singularity time as a function of initial amplitude. (b) Minimum interface height as a function of time.

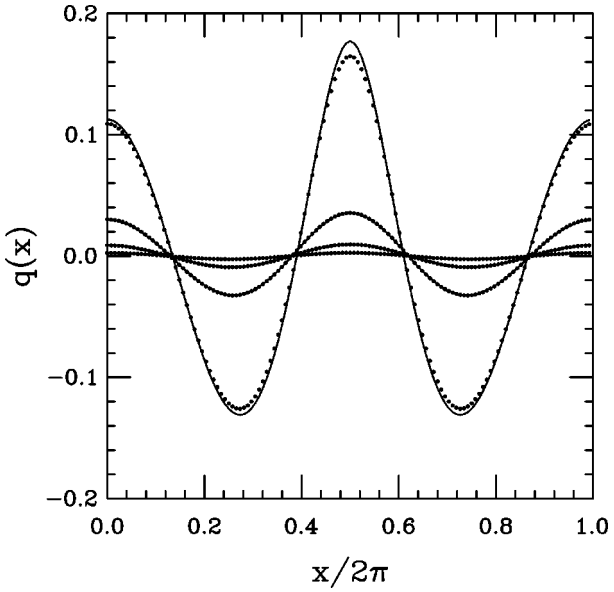

FIG. 21. Comparison between analytical correction function (solid) and numerical results (dotted) near the singularity.

preted as the collision on the real axis of two singularities, located at $\pi \pm i \ln|\lambda_-|$ in the complex x plane.

Observe also that the Fourier-space representation of $q(x)$ has the very simple form

$$q(x)=A(a)\sum_{n=2}^{\infty}(-1)^n\frac{\lambda_-^n}{n^3-n}\cos nx, \tag{102}$$

where $A(a)$ is a smooth function of the time-dependent amplitude $a(t)$. Since $\lambda_- \leqslant 1$, and equality holds only when $a=1$, the power-law spectrum of q is cutoff by an exponential factor whose range diverges to infinity as the low mode touches down. This is fully consistent with the asymptotic results of Eq. (82) and the numerical results described earlier.

One interesting point to note is that near the singularity time t_p and singularity point $x_p=\pi$, the asymptotic behavior of the correction function is not of scaling form $(t_p-t)^\alpha F((x-x_p)/(t_p-t)^\beta)$.

Until times very close to the singularity, full simulations show very good agreement between the form of the correction function (and its spectrum) with the asymptotic result (101). Figure 21 shows a comparison between the two in real space.

$m=2$: Here we choose

$$p=1+a(t)\cos x+b(t)\cos 2x. \tag{103}$$

This case is interesting for two main reasons. First, it allows us to examine a correction to the single mode truncation, where the $k=2$ mode now has its own independent dynamics. Second, beyond a threshold value of the bond number, it is possible to observe the development of two singularities instead of one.

Substitution into (92) yields two evolution equations for the amplitudes of the independent modes

$$\begin{pmatrix}\dot a\\ \dot b\end{pmatrix}=\frac{b}{\xi}\begin{pmatrix}1-\xi+\eta^2 & -\eta\\ -2\eta & 2\end{pmatrix}\begin{pmatrix}\frac{1}{2}(B-1)a\\ (B-4)b\end{pmatrix}, \tag{104}$$

where $\eta=\lambda_1+\lambda_2$ and $\xi=\lambda_1\lambda_2$ are both real. The four zeros (λ_i and λ_i^{-1}) are found as solutions to the pair of equations

$$\lambda^2-y\lambda+1=0,\quad \frac{b}{2}y^2+\frac{a}{2}y+(1-b)=0. \tag{105}$$

Let us now examine the two-dimensional (a,b) phase space as a function of B. This space is constrained by requiring that $p\geqslant 0$ and is reflection symmetric about $a=0$. Figure 22 shows the constrained domain. In the right half-plane ($a\geqslant 0$), the line $b=a-1$, for $-1\leqslant b\leqslant \frac{1}{3}$, defines those pinching configurations with a single touchdown at $x=\pi$. For

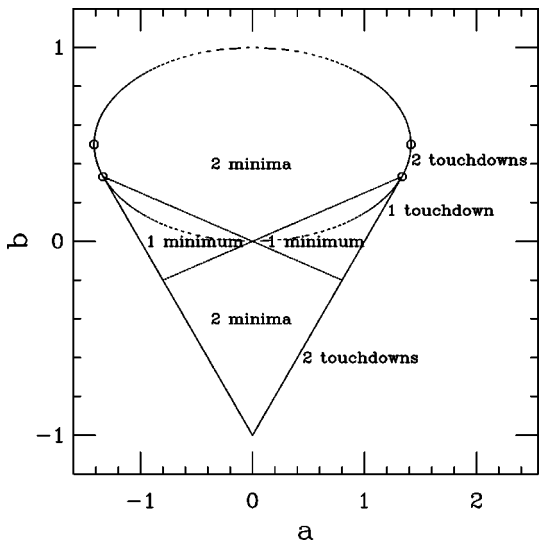

FIG. 22. Division of the phase domain for the two-mode approximation, indicating behavior of the interface.

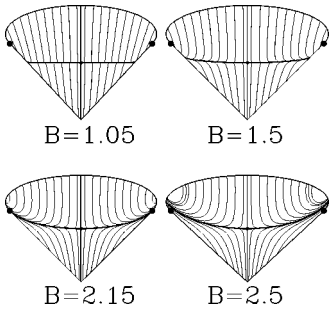

FIG. 23. Trajectories of solutions in the a-b phase domain for increasing bond number. Motion is towards and out along the curved unstable manifold.

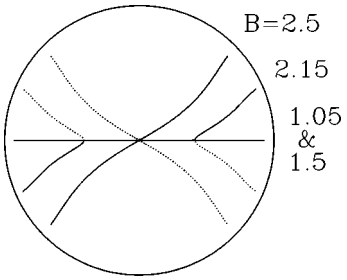

FIG. 24. Trajectories of zeros in the complex λ plane as a function of increasing bond number. Solid and dashed lines represent complex conjugate pairs. Motion is towards the unit circle.

$\frac{1}{3}<b<1$ the ellipse $a=[8b(1-b)]^{1/2}$ is the locus of configurations with two touchdowns. The function p is strictly positive in the interior of the ice cream cone-shaped region. This domain is divided by the line $b=a/4$ into regions where p has a single minimum and where it has two. The domain can also be divided in terms of the locations of the complex zeros λ_1 and λ_2 within the unit circle in the z plane. Within the ellipse defined above, $\lambda_1=\lambda_2^*$ and they are complex, while exterior to that ellipse both zeros lie on the real axis.

We focus now on the organization of the phase trajectories defined by Eq. (104). Linearization about the steady state $(a,b)=(0,0)$ gives $\dot{a}=(B-1)a$ and $\dot{b}=2(B-4)b$, as also found from linear analysis of the full PDE. Thus, for $B<1$ the point (0,0) is asymptotically stable. For $1<B<4$, the local stable manifold is the b axis, while the a axis is an unstable invariant manifold.

Figure 23 shows the (a,b) phase domain for $B=1.05$, 1.50, 2.15, and 2.50. Recall that a point on the domain boundary ($|\lambda|=1$) with $b<\frac{1}{3}$ has a single touchdown, while for $b>\frac{1}{3}$ there are two. The boundary point with $b=\frac{1}{3}$ is shown as a solid dot. For $B=1.05$, the unstable manifold to (0,0) is very flat across the phase domain, and its terminus lies on the domain boundary with b very slightly positive ($b\approx 0.008$). As for the $m=1$ case, intersection with the domain boundary gives a singularity in the evolution of the ordinary differential equation. It appears that any initial condition within the phase domain that is not upon the stable manifold will intersect the domain boundary within a finite time. Orbits are attracted strongly onto the unstable manifold, in accordance with our slaving picture; the unstable manifold is clearly the organizing structure of the phase flow.

As B is increased further, the unstable manifold bends upwards, and its terminus on the domain boundary also moves to larger values of b. At $B=\underline{B}\approx 2.1$, this terminus crosses $b=\frac{1}{3}$, and there is a bifurcation to two touchdowns. Figure 24 shows the motion of orbits of λ_1 (solid) and λ_2 (dashed when off the real axis) within the unit λ-circle. For small B ($B=1.05,1.5$) the unstable manifold maps completely onto the real λ-axis—i.e., the manifold lies entirely beneath the lower boundary of the ellipse. The two real zeros then evolve along the real axis, and one of these zeros moves out and collides with the unit circle, producing again a single touchdown. For $B>\underline{B}$, the unstable manifold crosses into the ellipse as the unit circle is approached. For $B=2.15$, the two initially real zeros collide at some time, and bifurcate off into the complex plane. Then they flow together as a conjugate pair towards the unit circle. The point of collision is where the unstable manifold crosses the ellipse. For $B=2.5$ the entire unstable manifold lies within the ellipse, and the two zeros evolve directly as conjugate pairs towards the unit circle. The presence of a conjugate pair would give a spectrum similar to that seen in Fig. 17. Examination of the numerical evidence suggests that $h_{\min}$ approaches zero linearly in time, as for the single mode case, and that $x_p(t)$ also approaches linearly to $x_p(t_p)$.

VI. CONCLUSIONS

In this work, we have developed an approximate analytical description of finite-time singularities in a class of viscous flows. Starting from the exact highly nonlocal vortex sheet description of interface motion in Hele–Shaw flow, we have developed a systematic procedure for generating equations of motion valid for asymptotically thin layers. This asymptotic limit is more tractable and retains many of the important features of the full problem, such as its conservation laws, linear stability properties, and variational structure.

We have focused on a dynamic that is intrinsically unstable, and thus for which a topological transition would appear to be inevitable. This Rayleigh–Taylor problem, with its simple competition between buoyancy and surface tension, has an underlying variational principle that allows us to prove that interface pinching must occur, at least in infinite time. The adjustable parameter that controls the instability (the bond number) may be tuned so that the unstable mode evolves arbitrarily slowly compared to all others. With this separation of time scales, and an associated partitioning of modes into ''active'' and ''slaved'', a systematic perturbation theory can be developed that leads to explicit expressions for the time evolution of all modes. Most importantly, these results constitute an approximate solution to the initial value problem. They predict quite accurately the singularity time observed in numerical studies of the full equation of motion. This partitioning of the modes can be generalized through the introduction of suitable projection operators, and can be recast naturally as the dynamics of zeros in the complex plane, a picture of singularity formation found in other systems as well.[25,38] Another natural question is whether

such techniques might be extended to the unforced ($B=0$) case, such as studied by Almgren *et al.*,[12] for which there is no apparent division of scales.

Many important unanswered questions remain for this class of problems, perhaps the most notable being how to prove that there is indeed finite-time pinching in the Rayleigh–Taylor problem. As well one would like a more rigorous understanding of the slaving analysis, perhaps using the techniques developed for proving the existence of inertial manifolds for dissipative PDEs. All of the results we have discussed pertain to finite systems in two dimensions, for which the spectrum of modes is discrete. One very natural issue is whether the slaving approximations developed here can be generalized to infinite systems with a continuous spectrum. Likewise, the extension of these ideas to more complicated free-surface flows remains an open problem. Examples include pattern formation through the nonlinear development of the Saffman–Taylor instability of an expanding gas bubble, and the Rayleigh instability of a fluid column or a soap film.[39] Finally, and on a more general level, we do not have a good understanding of how smooth large-scale flows induced by instabilities connect up with scaling solutions near singularities. This aspect appears to be central to the determination of singularity exponents in the scaling forms.

ACKNOWLEDGMENTS

We thank A. Bertozzi, R. Kohn, and most especially M. Pugh for helpful discussions. This work was supported in part by NSF PFF grant DMR93-50227 and DMR96-96257 and the A.P. Sloan Foundation (REG), by NSF PYI grant DMS-9396403, grant DMS-9404554, DOE grant DE-FG02-88ER25053, and by the Exxon Educational Foundation (MJS).

APPENDIX A: THE LUBRICATION EXPANSIONS

Here we show some of the technical details involved in the expansions of the vortex sheet integrals that lead to the lubrication equations of motion. This uses an asymptotic technique developed in Baker and Shelley[28] for studying thin vortex layers (Moore[40] used a matched asymptotics approach for this same problem). Generalizing the expression for the fluid velocity (6) to the case of two interfaces located at positions z_1 and z_2, the equation of motion for either is

$$\frac{\partial z_j^*}{\partial t}(p,t)=\frac{1}{2\pi i}P\int_{-\infty}^{+\infty}dp'\,\frac{\gamma_1(p')}{z_j(p)-z_1(p')}+\frac{1}{2\pi i}P\int_{-\infty}^{+\infty}dp'\,\frac{\gamma_2(p')}{z_j(p)-z_2(p')},\tag{A1}$$

where P means the principal value integral of the self-interaction term. Now let $Q^*(z_j)=\partial z_j^*/\partial t$. By the assumed symmetry of the interfaces, the vortex sheet strengths are equal in magnitude and opposite in sign and satisfy

$$\gamma+2A_\mu\,\mathrm{Re}\{z_p Q^*(z)\}=\partial_p(\kappa+B\phi(z)).\tag{A2}$$

The two interfaces are located at $x\pm i\epsilon h(x)$, and we seek expansions in ϵ of the vortex sheet strength

$$\gamma=\gamma^{(0)}+\epsilon\gamma^{(1)}+\epsilon^2\gamma^{(2)}+\cdots.\tag{A3}$$

This requires the calculation of expressions of the type

$$I_1-I_2=\frac{1}{2\pi i}\int_{-\infty}^{+\infty}\frac{\gamma(x')dx'}{(x-x')+i\epsilon h_+}-\frac{1}{2\pi i}P\int_{-\infty}^{+\infty}\frac{\gamma(x')dx'}{(x-x')+i\epsilon h_-},\tag{A4}$$

where $h_\pm=h(x)\pm h(x')$.

Of the two integrals I_1 and I_2, the former is the more difficult. The evaluation of I_2 involves geometric expansions of the integrand, together with integrations by parts, and is possible because the quantity $(h(p)-h(q))/(p-q)$ is bounded for smooth h. The unboundedness of the quantity $(h(p)+h(q))/(p-q)$ as $p-q\to 0$ renders the integral I_1 and its kindred more difficult. The coefficients of their Taylor expansions are instead obtained through a limiting procedure of the form

$$I_1(\epsilon)\simeq\lim_{\epsilon\to 0}I_1(\epsilon)+\epsilon\lim_{\epsilon\to 0}\frac{dI_1(\epsilon)}{d\epsilon}+\cdots.\tag{A5}$$

This procedure amounts to an application of the Plemelj formulas, and generates both local and nonlocal terms. After considerable algebra, we obtain

$$I_1[\gamma]-I_2[\gamma]=U[\gamma]-iV[\gamma],\tag{A6}$$

where

$$U[\gamma]=\sum_{m=0}^{\infty}\frac{(-1)^m\epsilon^{2m}}{2(2m)!}\frac{d^{2m}}{dx'^{2m}}\left(\gamma(x')h_+^{2m}\right)\Big|_{x'=x}+\sum_{m=0}^{\infty}\frac{(-1)^m\epsilon^{2m+1}}{2(2m+1)!}\mathscr{H}\left[\frac{d^{2m+1}}{dx'^{2m+1}}\{\gamma(x')\Delta^{2m+1}\}\right],\tag{A7}$$

where

$$\Delta^{2m+1}=h_+^{2m+1}-h_-^{2m+1},\tag{A8}$$

and

$$V[\gamma]=-\sum_{m=0}^{\infty}\frac{(-1)^m\epsilon^{2m+1}}{2(2m+1)!}\frac{d^{2m+1}}{dx'^{2m+1}}\left(\gamma(x')h_+^{2m+1}\right)\Big|_{x'=x}+\sum_{m=0}^{\infty}\frac{(-1)^m\epsilon^{2m}}{2(2m)!}\mathscr{H}\left[\frac{d^{2m}}{dx'^{2m}}\{\gamma(x')\Delta^{2m}\}\right].\tag{A9}$$

Noting that $\mathrm{Re}\{(\partial_p z_2)Q^*\}=U+V\epsilon h_x$ in Eq. (A2), and substituting from (A3) we obtain

$$U+V\epsilon h_x\simeq\tfrac{1}{2}\gamma^{(0)}+\epsilon(\tfrac{1}{2}\gamma^{(1)}+\mathscr{H}[\{\gamma^{(0)}h\}_x])+\epsilon^2(\tfrac{1}{2}\gamma^{(2)}+\mathscr{H}[\{\gamma^{(1)}h\}_x]-\partial_x(h\partial_x(h\gamma^{(0)})))+\cdots.\tag{A10}$$

The right-hand side of (A2) has also an expansion in ϵ

$$\partial_x(\kappa+B\phi(z_2))=P^{(0)}+\epsilon P^{(1)}+\epsilon^2P^{(2)}+\cdots,\tag{A11}$$

whose coefficients $P^{(n)}$ depend only on the function h, its spatial derivatives, and the parameter B. Then order by order in ϵ (A2) becomes

$$\begin{aligned} P^{(0)} &= (1+A_\mu)\gamma^{(0)}, \\ P^{(1)} &= (1+A_\mu)\gamma^{(1)} + 2A_\mu \mathscr{H}[\{\gamma^{(0)}h\}_x], \\ P^{(2)} &= (1+A_\mu)\gamma^{(2)} + 2A_\mu \mathscr{H}[\{\gamma^{(1)}h\}_x] \\ &\quad - 2A_\mu \partial_x(h\partial_x(h\gamma^{(0)})). \end{aligned} \tag{A12}$$

Solving this order by order in ϵ yields the functions $\gamma^{(n)}$

$$\begin{aligned} \gamma^{(0)} &= \frac{1}{1+A_\mu} P^{(0)}, \\ \gamma^{(1)} &= \frac{1}{1+A_\mu} P^{(1)} - \frac{2A_\mu}{1+A_\mu} \mathscr{H}[\{P^{(0)}h\}_x], \end{aligned} \tag{A13}$$

and so on.

Finally, the equation of motion for the interface takes the general form

$$\begin{aligned} h_t = -\partial_x\{h(\gamma^{(0)} + \epsilon\gamma^{(1)} + \epsilon^2\gamma^{(2)} + \epsilon\gamma^{(0)}\mathscr{H}[h_x] \\ + \epsilon^2\mathscr{H}[(\gamma^{(1)}h)_x] - \epsilon^2\gamma^{(0)}(hh_x)_x + \cdots)\}. \end{aligned} \tag{A14}$$

APPENDIX B: A PERTURBATIVE APPROACH TO TOUCHDOWN SINGULARITIES

In this Appendix, we present two examples of a perturbative approach to understanding touchdown singularities. In each case, we again exploit the existence of a slow time scale. The first example is the Rayleigh–Taylor problem, with $B=1+\epsilon$ for $\epsilon \ll 1$. Rescaling time as in Eq. (73), the lubrication equation reads

$$\epsilon h_\tau = -\partial_x(h(\mathscr{L}_1 h + \epsilon h_x)). \tag{B1}$$

We assume that h can be expanded in ϵ as

$$h = \xi^0 + \epsilon\xi^1 + \cdots. \tag{B2}$$

At $O(1)$ in this expansion, we have

$$-\partial_x(\xi^0 \mathscr{L}_1 \xi^0) = 0. \tag{B3}$$

It is straightforward to show that with periodic boundary conditions

$$\xi^0 = 1 + a(t)\cos x. \tag{B4}$$

While $\sin x$ is also in the null space of $\mathscr{L}_1$, it can be subsumed into the above form through a phase shift. As before, the time dependence in a is determined by a solvability condition that allows a continuation of the asymptotic expansion. At the next order we have the shallow-water form

$$\xi^0_\tau = -\partial_x(\xi^0(\mathscr{L}_1\xi^1 + \xi^0_x)). \tag{B5}$$

Again, if $\xi^0 \to 0$ then ξ^1 must develop a singularity. This equation can be integrated up once, and written as a differential equation for ξ^1

$$\mathscr{L}_1\xi^1 = -\frac{\tilde{\xi}^0_\tau}{\xi^0} - \xi^0_x \equiv \mathscr{R}. \tag{B6}$$

To solve for ξ^1, the Fredholm Alternative must be satisfied. There are three independent solutions to $\mathscr{L}_1\psi = 0$: $\psi_1 = 1$, $\psi_2 = \cos x$, $\psi_3 = \sin x$. Thus, to find a solution to Eq. (B6), it must be that

$$\langle \mathscr{R}, \psi_1 \rangle = \langle \mathscr{R}, \psi_2 \rangle = \langle \mathscr{R}, \psi_3 \rangle = 0, \tag{B7}$$

are satisfied, where $\langle \cdot, \cdot \rangle$ is the usual $L^2[0,2\pi]$ inner product. The first two are trivially satisfied, the last is not. One verifies by direct integration that the last condition reproduces the equation of motion for the amplitude $a(\tau)$ found in Eq. (94).

As mentioned above, this has further implications for ξ^1. Applying the solvability condition, that is, the ODE for a, gives

$$\mathscr{L}_1\xi^1 = \frac{1}{2} a \frac{(1-\sqrt{1-a^2}) + 2a\cos x}{1 + a\cos x} \sin x. \tag{B8}$$

Integration of this equation for ξ^1 gives the expression found for q in Eq. (101). As $a \to 1^-$, the right-hand-side acquires a pole singularity at $x=\pi$. The local behavior of $\mathscr{L}_1\xi^1$ can be rewritten in a scaling form

$$\mathscr{L}_1\xi^1 \simeq \frac{1}{\sqrt{\tau_p - \tau}} \frac{\eta}{1+\eta^2}, \quad \eta = \frac{x-\pi}{\sqrt{\tau_p - \tau}}. \tag{B9}$$

This implies that ξ^1_{xx} diverges as $\tau \to \tau_p$.

In our second example, we apply this asymptotic approach to a thin layer of liquid pinching under a slow outflux of fluid. We consider the lubrication equation with surface tension alone

$$h_t = -\partial_x(hh_{xxx}), \tag{B10}$$

but with the modified boundary conditions

$$h(1,t) = 1, \quad h_{xxx}(1,t) = \epsilon \ll 1, \tag{B11}$$

with h even about $x=0$. The mass flux is hh_{xxx}, and so these boundary conditions at $x=1$ correspond to an imposed, slow outflux of liquid from the layer.

We expand h as in Eq. (B2), and again rescale time as $\tau = \epsilon t$. At first order we find

$$-\partial_x(\xi^0\xi^0_{xxx}) = 0, \tag{B12}$$

with the boundary conditions

$$\xi^0(1,\tau) = 1, \quad \xi^0_{xxx}(1,\tau) = 0, \tag{B13}$$

and ξ^0 even about $x=0$. This yields

$$\xi^0(x,t) = 1 + a(\tau)(x^2 - 1), \tag{B14}$$

where $a(\tau)$ is determined at next order. At $O(\epsilon)$ we have

$$a_\tau(x^2-1) = -\partial_x(\xi^0\xi^1_{xxx}), \tag{B15}$$

with ξ^1 even about $x=0$ and

$$\xi^1(1,\tau) = 0, \quad \xi^1_{xxx}(1,\tau) = 1. \tag{B16}$$

Integrating up once, and using eveness at $x=0$, gives

$$a_\tau(\tfrac{1}{3}x^2 - x) = -\xi^0\xi^1_{xxx}. \tag{B17}$$

Where before we applied a solvability condition to determine $a(\tau)$, we now use boundary conditions. Applying the boundary conditions at $x=1$ on $\xi^{0,1}$, we find

$$a(\tau)=\tfrac{3}{2}\tau+a_0, \tag{B18}$$

which gives a time $\tau_p=(\frac{2}{3})(1-a_0)$ when the zeroth-order solution pinches. As before, this has consequences for the next order correction ξ^1. Namely, Eq. (B15) becomes

$$\xi^1_{xxx}=-\frac{3}{2}\frac{\frac{1}{3}x^3-x}{1+a(\tau)(x^2-1)}, \tag{B19}$$

and at the pinch time

$$\xi^1_{xxx}=-\frac{3}{2}\frac{\frac{1}{3}x^2-1}{x}, \tag{B20}$$

which has a pole singularity at $x=0$. Once again, ξ^1_{xx} is logarithmically divergent at the pinching time.

APPENDIX C: PROPERTIES OF DECOUPLED SLAVING APPROXIMATION

In this section, we prove several properties of the alternative slaving system (85)

$$p_t=y_x, \quad \mathscr{P}_m\frac{y}{p}=-\mathscr{L}p.$$

We first prove that $\mathscr{P}_m p^{-1}$ is symmetric and positive definite in $\mathbf{L}^2[0,2\pi]$. Let $\mathbf{P}^m$ be the set of real valued, finite Fourier polynomials of order m, i.e., $\mathbf{P}^m=\{r(x)|\mathscr{P}_m r=r\}$. The inner product of any two polynomials in $\mathbf{P}^m$ will be defined as the usual $\mathbf{L}^2[0,2\pi]$ inner product.

Lemma: The operator $\mathscr{P}_m p^{-1}$: $\mathbf{P}^m\to\mathbf{P}^m$, for $p>0$ smooth and periodic, is a symmetric and positive definite operator.

This follows directly from the simple statement that any $w\in\mathbf{P}^m$ is orthogonal to $\mathscr{Q}_m v$ for any v periodic and smooth. That is,

$$\int_0^{2\pi}dx w(x)v(x)=\int_0^{2\pi}dx w(x)(\mathscr{P}_m v)(x). \tag{C1}$$

Then given r, $s\in\mathbf{P}^m$

$$\int_0^{2\pi}dx r(x)\left(\mathscr{P}_m\frac{s}{p}\right)(x)=\int_0^{2\pi}dx\,\frac{1}{p(x)}\,r(x)s(x)$$
$$=\int_0^{2\pi}dx s(x)\left(\mathscr{P}_m\frac{r}{p}\right)(x), \tag{C2}$$

which shows symmetry. Positive definiteness follows by setting $r=s$.

We now show that $\mathscr{F}[p]$ and $\mathscr{S}[p]$, as defined by Eqs. (21) and (23), serve as energy and entropy for the system (85).

Theorem: Let $p\in\mathbf{P}^m$ be a solution to system (85). Then,

$$\frac{d}{dt}\mathscr{F}[p]=\frac{d}{dt}\frac{1}{2}\int_0^{2\pi}dx(p_x^2-Bp^2)$$
$$=-\int_0^{2\pi}dx p\left(\frac{y}{p}\right)^2<0, \tag{C3}$$

$$\frac{d}{dt}\mathscr{S}[p]=\frac{d}{dt}\left(-\int_0^{2\pi}dx f(x)\ln f(x)\right)$$
$$=\frac{1}{h}\int_0^{2\pi}dx(p_{xx}^2-Bp_x^2), \tag{C4}$$

where $f=p/\overline{p}$, and $y_x=p_t$.

Beginning with the energy, we have

$$\frac{d}{dt}\mathscr{F}=\int_0^{2\pi}dxy\mathscr{L}_B p=-\int_0^{2\pi}dxy\mathscr{P}_m\frac{y}{p}, \tag{C5}$$

$$=-\int_0^{2\pi}dxy\frac{y}{p}=-\int_0^{2\pi}dxp\left(\frac{y}{p}\right)^2. \tag{C6}$$

The first line of equalities are obvious. The last line follows from the fact that for any $a\in\mathbf{P}^m$, and smooth, periodic b

$$\int_0^{2\pi}dxab=\int_0^{2\pi}dxa(\mathscr{P}_m+\mathscr{Q}_m)b$$
$$=\int_0^{2\pi}dxa\mathscr{P}_m b. \tag{C7}$$

The identity for the entropy follows in a similar fashion.

[1] M. F. Shatz, S. J. VanHook, W. D. McCormick, J. B. Swift, and H. L. Swinney, ''Onset of surface-tension-driven Benard convection,'' Phys. Rev. Lett. **75**, 1938 (1995), and references therein.

[2] M. A. Lewis, ''Spatial coupling of plant and herbivore dynamics: The contribution of herbivore dispersal to transient and persistent ''waves'' of damage,'' Theor. Pop. Biol. **45**, 277 (1994).

[3] A. T. Dorsey and R. E. Goldstein (unpublished).

[4] J. R. King, ''The isolation oxidation of silicon: the reaction-controlled case,'' SIAM (Soc. Ind. Appl. Math.) J. Appl. Math. **49**, 1064 (1989).

[5] G. Tryggvason and H. Aref, ''Numerical experiments on Hele-Shaw flow with a sharp interface,'' J. Fluid Mech. **136**, 1 (1983).

[6] R. E. Goldstein, A. I. Pesci, and M. J. Shelley, ''Topology transitions and singularities in viscous flows,'' Phys. Rev. Lett. **70**, 3043 (1993).

[7] R. E. Goldstein, A. I. Pesci, and M. J. Shelley, ''Attracting manifold for a viscous topology transition,'' Phys. Rev. Lett. **75**, 3665 (1995).

[8] P. Constantin, T. F. Dupont, R. E. Goldstein, L. P. Kadanoff, M. Shelley, and S.-M. Zhou, ''Droplet breakup in a model of the Hele-Shaw cell,'' Phys. Rev. E **47**, 4169 (1993).

[9] T. F. Dupont, R. E. Goldstein, L. P. Kadanoff, and S.-M. Zhou, ''Finite-time singularity formation in Hele-Shaw systems,'' Phys. Rev. E **47**, 4182 (1993).

[10] A. L. Bertozzi, ''Symmetric singularity formation in lubrication-type equations for interface motion,'' SIAM (Soc. Ind. Appl. Math.) J. Appl. Math. **56**, 681 (1996).

[11] A. L. Bertozzi, M. P. Brenner, T. F. Dupont, and L. P. Kadanoff, in *Centennial Edition, Applied Mathematics Series*, edited by L. Sirovich (Springer-Verlag, New York, 1993).

[12] R. Almgren, A. Bertozzi, and M. Brenner, ''Stable and unstable singularities in the unforced Hele-Shaw cell,'' Phys. Fluids **8**, 1356 (1996).

[13] A. Bertozzi and M. Pugh, ''The lubrication approximation for thin viscous films: Regularity and long time behavior of weak solutions,'' Commun. Pure Appl. Math. **49**, 85 (1996).

[14] A. Bertozzi and M. Pugh, ''Long-wave instabilities and saturation in thin film equations,'' Commun. Pure Appl. Math. **51**, 625 (1998).

[15]R. Almgren, ''Singularity formation in Hele-Shaw bubbles,'' Phys. Fluids **8**, 344 (1996).
[16]F. Otto, ''Lubrication approximation with prescribed non-zero contact angle: an existence result,'' to appear in Comm. Partial Diff. Eqs. (1998).
[17]S. Cardoso and A. Wood, ''The formation of drops through viscous instability,'' J. Fluid Mech. **289**, 351 (1995).
[18]J. Eggers, ''Universal pinching of 3D axisymmetric free-surface flow,'' Phys. Rev. Lett. **71**, 3458 (1993); J. Eggers and T. F. Dupont, ''Drop formation in a one-dimensional approximation of the Navier-Stokes equation,'' J. Fluid Mech. **262**, 205 (1994).
[19]X. D. Shi, M. P. Brenner, and S. R. Nagel, ''A cascade of structure in a drop falling from a faucet,'' Science **265**, 219 (1994); M. P. Brenner, X. D. Shi, and S. R. Nagel, ''Iterated instabilities during droplet formation,'' Phys. Rev. Lett. **73**, 3391 (1994).
[20]S. Bechtel, C. D. Carlson, and M. G. Forest, ''Recovery of the Rayleigh capillary instability from slender 1-D inviscid and viscous models,'' Phys. Fluids **12**, 2956 (1995).
[21]D. Papageorgiou, ''On the break-up of viscous liquid threads,'' Phys. Fluids **7**, 1529 (1995).
[22]M. Brenner, J. Lister, and H. Stone, ''Pinching threads, singularities and the number 0.0304...,'' Phys. Fluids **8**, 2827 (1996).
[23]M. Pugh and M. Shelley, ''Singularity formation in models of thin jets,'' to appear in Comm. Pure and Appl. Math. (1998).
[24]P. Constantin, C. Foias, R. Temam, and B. Nicolaenko, *Integral and Inertial Manifolds for Dissipative PDEs* (Springer, Berlin, 1988).
[25]B. I. Shraiman and D. Bensimon, ''Singularities in nonlocal interface dynamics,'' Phys. Rev. A **30**, 2840 (1984); P. Constantin and L. P. Kadanoff, ''Dynamics of a complex interface,'' Physica D **47**, 450 (1991); S. Tanveer, ''Evolution of Hele-Shaw interface for small surface tension,'' Philos. Trans. R. Soc. London, Ser. A **343**, 155 (1993).
[26]G. R. Baker, D. I. Meiron, and S. A. Orszag, ''Generalized vortex methods for free-surface flow problems,'' J. Fluid Mech. **123**, 477 (1982).
[27]T. Y. Hou, J. S. Lowengrub, and M. J. Shelley, ''Removing the stiffness from interfacial flows with surface tension,'' J. Comput. Phys. **114**, 312 (1994).
[28]G. R. Baker and M. J. Shelley, ''On the relation between thin vortex layers and vortex sheets,'' J. Fluid Mech. **215**, 161 (1991).
[29]M. J. Shelley (unpublished).
[30]Y. Saad and M. R. Schultz, ''GMRES: A generalized minimum residual method for solving nonsymmetric linear systems,'' SIAM (Soc. Ind. Appl. Math.) J. Sci. Stat. Comput. **7**, 856 (1986).
[31]M. Shelley, ''A study of singularity formation in vortex sheet motion by a spectrally accurate vortex method,'' J. Fluid Mech. **244**, 493 (1992).
[32]R. Krasny, ''A study of singularity formation in a vortex sheet by the point vortex approximation,'' J. Fluid Mech. **167**, 65 (1986).
[33]C. Sulem, P. L. Sulem, and H. Frisch, ''Tracing complex singularities with spectral methods,'' J. Comput. Phys. **50**, 138 (1983).
[34]A. Bertozzi (private communication).
[35]W. Magnus and S. Winkler, *Hill's Equation* (Dover, New York, 1979).
[36]C. M. Bender and S. A. Orszag, *Advanced Mathematical Methods for Scientists and Engineers* (McGraw-Hill, New York, 1978).
[37]M. S. Jolly, I. G. Kevrekidis, and E. S. Titi, ''Preserving dissipation in approximate inertial forms for the Kuramoto-Sivashinsky equation,'' J. Diff. Eqns. **3**, 179 (1991); Also C. Foias, M. S. Jolly, I. G. Kevrekidis, and E. S. Titi, ''On some dissipative fully discrete nonlinear Galerkin schemes for the Kuramoto-Sivashinsky equation,'' Phys. Lett. A **186**, 87 (1994).
[38]D. W. Moore, ''The spontaneous appearance of a singularity in the shape of an evolving vortex sheet,'' Proc. R. Soc. London, Ser. A **365**, 105 (1979).
[39]S. A. Cryer and P. H. Steen, ''Collapse of the soap-film bridge: quasistatic description,'' J. Colloid Interface Sci. **154**, 276 (1992); Y.-J. and Chen and P. H. Steen, ''Dynamics of inviscid capillary breakup: collapse and pinchoff of a film bridge,'' J. Fluid Mech. **341**, 245 (1997).
[40]D. W. Moore, ''The equation of motion of a vortex layer of small thickness,'' Stud. Appl. Math. **58**, 119 (1978).